공학박사학위논문

고성능 한계 핸들링을 위한 인휠 모터 토크벡터링 제어

Torque Vectoring Control of In-Wheel Motor Vehicles for Dynamic Limit Handling

August 2021

서울대학교 대학원

기계항공공학부

현 영 진

고성능 한계 핸들링을 위한 인휠모터 토크벡터링 제어

Torque Vectoring Control of In-Wheel Motor Vehicles for Dynamic Limit Handling

지도교수 이 경 수

이 논문을 공학박사 학위논문으로 제출함

2021 년 4 월

서울대학교 대학원

기계항공공학부

현 영 진

현영진의 공학박사 학위논문을 인준함

2021 년 6 월

위 원 장 : 이 동 준

부위원장 : 이 경 수

위 원 : 송 한 호

위 원 : 이 재 완

위 원 : 박 준 홍

Abstract

Torque Vectoring Control of In-Wheel Motor Vehicles for Dynamic Limit Handling

Youngjin Hyun

School of Mechanical and Aerospace Engineering

The Graduate School

Seoul National University

In the last ten decades, vehicle stability control systems have been dramatically developed and adapted in many commercial vehicles to avoid fatal crashes. Significantly, ESC (Electric Stability Control) system can help escape the accident from unstable driving conditions with dangerous roads such as slippery roads due to inclement weather conditions. However, for the high performed vehicle, frequent intervention from ESC reduces the pleasure of fun-to-drive. Recently, the development of traction control technologies has been taking place with that of the electrification of vehicles. The IWMs (In-Wheel Motor system), which is one of the systems that can apply independent drive of each wheel, for the limit handling characteristics, which are the operation areas of the ESC, is introduced for the control that enables the lateral characteristics of the vehicle dynamics. Firstly, the automated drift control algorithm can be proposed for the nonlinear limit handling condition of vehicles. This approach can give an insight of fun-to-drive mode to TV (Torque Vector) control scheme, but also the stability control of high sideslip angle of the vehicle on slippery roads. Secondly, using IWMs system with front two motors, understeer

gradient of vehicle, which is the unique characteristics of vehicle can be used for the proposed control strategy. A new transient parameter is formulated to be acquired rapid response of controller and reducing chattering effects. Simulation and vehicle tests are conducted for validation of TV control algorithm with steady-state and transient ISO-based tests. Finally, dynamic torque vectoring control with a four-wheel motor system with Multiple Adaptive Sliding Mode Control (MASMC) approach, which is composed of a yaw rate controller and sideslip angle controller, is introduced. Highly nonlinear characteristics, cornering stiffnesses of front and rear tires are estimated by adaptation law with measuring data. Consequently, there are two types of driving modes, the safety mode and the dynamic mode. MASMC algorithm can be found and validated by simulation in torque vectoring technology to improve the handling performance of fully electric vehicles.

Keywords: Torque Vectoring Control, Autonomous driving system, Automated drifting control, Multiple adaptive sliding mode control, In-wheel motor system.

Student Number: 2016-35616

List of Figures

Contents

Chapter 1 Introduction

1.1. Background and Motivation

For the automotive industry, torque vectoring (TV) is a modern concept to enhance driving stability and safety whilst improving vehicle dynamics and the fun-to-drive [Knauder et al. 2014]. Furthermore, Investigating the recent technology trends in the automobile industry, vehicle applications of technologies such as electrification and autonomous driving of modern passenger cars are actively progressing. Vehicle chassis control technology can be a role to improve driving safety and high skilled handling performance along with advances in electrification and autonomous driving technology. In particular, the chassis control platform that can independently drive and brake four wheels according to electrification, can improve driving function and performance through new approaches with control technologies. Moreover, the use of multiple motors on the vehicle allows, for example, the allocation of one motor per wheel. This makes it possible to control each wheel independently, and it becomes easy to apply torque-vectoring-based control strategies [Dizqah et al. 2016].

Stability control of vehicles has been researched for many decades [Van Zanten 2002]. Most of these researches [Van Zanten 2002, Koibuchi et al. 1996, Abe et al. 1999, Williams and Haddad 1995, David 2004] detect the vehicle instability with the difference between actual and desired yaw rate and utilize differential braking to stabilize the vehicle (or minimize the sideslip angle of the vehicle). The output of these researches is now commercialized and equipped in vehicles as ESC (Electric Stability Control) system. This system can provide excellent benefits on accident avoidance of emergency with

instability of vehicle on high or low friction roads. However, another point of view, in recent years, with the development of vehicle technology, the driving performance of the vehicle has been gradually increased and the performance of the vehicle has been improved, and thus providing the pleasure of driving to customers is also emerging as an important commercial value. To provide fun-to-drive or sporty driving feels on passenger car, some OEM carmakers have developed and applied a system to reduce or minimize ESC intervention by matching the ESC operation strategy to the driving mode, or to select the ESC-OFF to the driver [Vossler 2014].

Basically, the ESC system secures stability by inducing the vehicle from an unstable to a stable state or a linear region on driving condition using the yaw moment using the vehicle's braking force. In addition, when excessive understeer occurs, the ESC is implemented to reduce the speed of the vehicle by limiting the driving force resulting from the power of the vehicle. As a result, the ESC system is controlled in the direction of increasing the braking force or reducing the driving force in order to secure the stability of the vehicle, and thus the loss of the vehicle speed is inevitable. Moreover, when ESC is activated, uncomfortable noise and vibration are generated due to the control limitation of hydraulic brake system. This is also a factor that hurts the ride comfort of the vehicle. Therefore, the torque vectoring technology using the braking force of the ESC cannot be actively applied to vehicles such as TVBB (Torque Vectoring By Brake), and the effect of TVBB is weak points, which is a reality that does not receive good evaluation in the market [Gluckman 2010].

TV(Torque Vectoring) originally is a technology employed in automobile mechanical differentials. A differential transfers engine torque to the wheels. TV technology provides the differential with the ability to vary the torque to

each wheel. This allows for the wheels to grip the road for better launch and handling [Ireson 2010]. The torque vectoring offers the ability to distribute the torque of the wheels individually and has a direct impact on the yaw moment

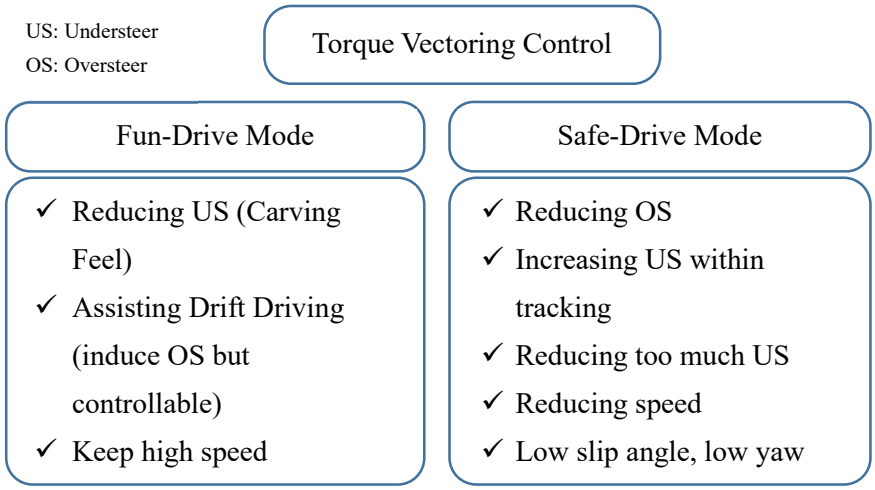

Figure 1.1 Function of torque vectoring control

of the vehicle. In conventional powertrain architectures, ESC generally relies on friction brakes, while TV differentials are rare due to their complexity and, as a result, higher costs. Electric vehicles with individual wheel-motor devices on top of each other allow selective torque distribution [Knauder et al. 2014]. The core control function of the TV control uses yaw moment controller, which brings a stable attitude and improved handling performance of the vehicle. Each wheel, exerted traction force, front and rear, left and right wheel, can give a rise to yaw moment which causes a steering vector of vehicle. Therefore, since it can control the yaw motion of the vehicle, it is able to be designed to contribute to the cornering function the vehicle as shown in Figure 1.1. In the fun drive mode, it is possible to create a function that reduces the understeer characteristic and, rather, generates intentional oversteer to enable drift driving.

It is also important to maintain high speed without slowing down. On the other hand, in the safe drive function, the oversteer which can be tricky to control to normal drivers, should be reduced as much as possible, and the occurrence of too much understeer than the driving direction is a factor that threatens stability, so this should also be reduced.

Figure 1.2 shows the range in which the electronic control systems of the functional unit that can give yaw motion while driving the vehicle affect the dynamic characteristics of the vehicle. In a turning situation, ESC helps maintain vehicle stability by limiting the engine's power or applying brakes to one or more of the wheels. These systems are advantageous from the standpoint of improving vehicle stability but are disadvantageous from a fun-to-drive point of view, independent of the driver's intention, because they reduce the vehicle's longitudinal speed by using engine power limitation and brakes. For active TV

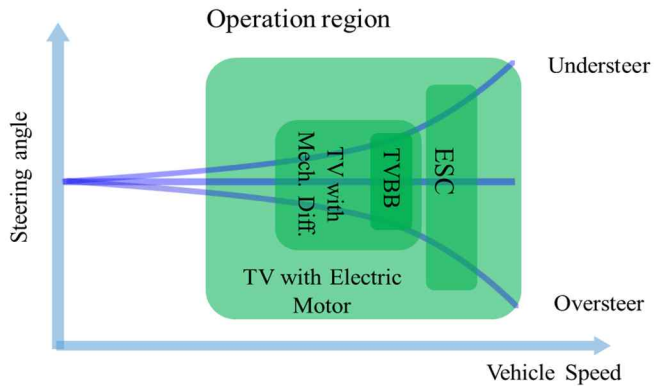

Figure 1.2 Range of action of various TV system

with differentials, a clutch can be a role to control the direction and amount of torque transmission to the wheel from the inside to the outside or from the outside to the inside of the turning to suppress the occurrence of understeer and oversteer depending on the situation.

In recent years, research on a torque vectoring system capable of regenerative braking using a motor and independently controlling left and right torques has been actively conducted. When using a motor, it is advantageous to apply torque vectoring technology by utilizing the motor's fast response characteristics and wide control area. As shown in Figure 1.2, a wider control range and 100% left and right independent control is possible than an active differential device, and it has the advantage of being able to control in finer understeer and oversteer areas than the braking system method using brake or ESC. Therefore, when applying a TV to an electric vehicle using an electric motor, if regenerative braking and elaborate control technology are used, the role of the ESC system can be reduced or deleted, resulting in cost reduction. TV control requires considering dynamic characteristics of the vehicle. This paper describes the study and control methods of non-linear characteristics of controlling the behavior of the vehicle in limit conditions when handling or cornering the vehicle.

1.2. Literature review

Stability control of vehicles with braking and traction in ICE has been researched for many decades[Van Zanten 2002]. Most of these researches[Van Zanten 2002, Koibuchi et al. 1996, Abe et al. 1999, Williams and Haddad 1995, David 2004], detect the vehicle instability with the difference between actual and desired yaw rate and utilize differential braking to stabilize the vehicle (or minimize the sideslip angle of the vehicle). The output of these researches such as ESC or VDC is now commercialized and equipped in vehicles by law. As described in the previous section, the electrification of vehicle causes major

change in the vehicle stability control system in terms of vehicle dynamics. This change is due to electric motor characteristics which have rapid response, low inertia, and accurate control, compared conventional ICE. Furthermore, at limit handling conditions, it is difficult to have the alteration of vehicle dynamic states due to restricted control inputs, such as engine torque and steering system. Firstly, the automated drift driving controls associated with the vehicle's limit handling are examined and which affect the fun to drive characteristics. The controller for autonomous drifting at limit handling condition has been developed and experimentally validated based on the equilibrium analysis in [Voser, Hindiyeh, and Gerdes 2010, Hindiyeh and Christian Gerdes 2014]. The online drift controller was designed based on the vehicle lateral dynamics and experimentally validated the controller [Voser, Hindiyeh, and Gerdes 2010]. The algorithm was expanded to include the vehicle longitudinal dynamics with electric motors [Hindiyeh and Christian Gerdes 2014]. These two researches play a key role to enlighten the fields of a controller design for automated drift. By using the study, The controller for autonomous racing by means of nonlinear model predictive control was designed [Liniger, Domahidi, and Morari 2015]. The controller to stabilize both vehicle dynamics and path tracking dynamics was proposed [Goh and Gerdes 2016]. In these papers, the controllers with electric vehicle are easier and flexible to control than a proposed controller in this dissertation with ICE powertrains which more restricted in terms of inputs to the controller. In Chapter 2, Automated drift is delt with limit handling control for advanced TV control including fun to drive mode with drifting technique. In recent research area of robotics, learning-based method, reinforcement learning, one of machine learning techniques, can be adapted in autonomous drifting control. Cutler et al. introduce a framework that combines

simple and complex simulators with a real-world remote-controlled car to realize a steady-state drift with constant sideways velocity, in which a model-based reinforcement learning algorithm, PILCO, is adopted [Cutler and How 2016]. A correction method of oversteering in high speed, using simulation-based reinforced learning, trajectories of driving and correction of oversteering (short drifting) are proposed in virtual environment [Cai et al. 2020]. For autonomous racing driving algorithm, it has been shown that the deep reinforcement learning algorithm made a fastest path to driving in racing circuits better than racing drivers with drifting effects in computer game program [Fuchs et al. 2021]. These studies can be a good insight for the autonomous drifting control of real vehicles, but enormous learning data is still required, and it is difficult to be tested in terms of safety for actual vehicles.

For TV controls, some researches have been conducted to improve the lateral motion and cornering performance of the vehicle using the in-wheel motors. One of the conventional approaches for the lateral motion control is to design and track a desired yaw rate [Kaiser et al. 2011, Nam, Fujimoto, and Hori 2015]. In [Kaiser et al. 2011], a linear quadratic Gaussian controller is designed to track the reference value of yaw rate and side slip angle with a feedback and feedforward control. In [Nam, Fujimoto, and Hori 2015], an adaptive sliding mode controller is devised to handle the parameter uncertainty of the vehicle model using the parameter adaptation law with tracking the yaw rate reference. A paper for TV control strategy for IWMs with steady-state and transient each [Vignati, Sabbioni, and Tarsitano 2016], similar approach of this paper, presented a controller which couples a LQR with offline yaw index which is directly related to oversteer and understeer behaviour of the vehicle. The yaw index depends on the sign of side slip angle and calculated yaw rate from lateral

acceleration. The understeer and oversteer can be decided by yaw index in steady-state conditions, but in transient condition, time-variant system, the yaw index does not have the variables depend on the parameters related with time. It means that the controller is considered as having some limitation on transient condition. Therefore, a proposed controller in Chapter 3 for IWMs, is designed by separately steady-state and transient terms in related equations for better performance.

To design a controller with satisfaction between safety mode and fun-to-drive mode, model predictive control scheme was used for actuating an active steering system to limit the vehicle side-slip angle in emergency situations [Beal and Gerdes 2012]. One type of solution to realize Fun to Drive for the common driver is by providing safe drifting capacity, as used by skilled drivers. Drifting is related to large side-slip angles (i.e. when the saturation of driving force occurs), and this makes controller design more difficult than safe driving, which is characterized by small side-slip angles and linear friction tire properties [Mutoh, Kazama, and Takita 2006], [Nam et al. 2012]. To control large side-slip angles, torque vectoring, which is also called yaw moment control, is primarily used by the distribution of the wheel torque individually. In [Lu et al. 2016], the integrated control method of yaw rate and side-slip angle control was presented for realizing the effective torque vectoring. However, the integrated and continuous control systems may be lost stability in unfavourable driving conditions due to different dynamic characteristics between yaw rate and side-slip angle.

1.3. Thesis Objectives

This dissertation focused on improving the handling performance at limit driving condition using traction and steering control algorithm with in-wheel motor systems. Analyzing the behavior of the vehicle in cornering limitations and developing a controller that can be tracked with vehicle states in the slipping on roads using the variation of steering angle and drive torque in directly. A new proposed TV control algorithm with vehicle dynamic characteristic, the understeer gradient-based control technique, is formulated for IWMs. The control scheme with steady-state and transient terms is successfully simulated and tested for validations with severe test scenarios. For four motor IWMs, cascaded multi adaptive sliding mode control algorithm is also proposed for robustness and uncertainties of the steering and traction parameters to adapt external tire forces. Finally, the four traction forces are distributed by an optimal control technique with constraints. The controller is also validated by full car simulation with several test scenarios.

1.4. Thesis Outline

This dissertation is structured in the following manner. Basic modelling and analysis of vehicle dynamics for limit driving conditions, handling and cornering of the vehicle are described in Chapter 2. In Chapter 3, using an In-Wheel Motor system (IWMs) applied to the real passenger vehicle, a new proposed TV controller is implemented with analysis of function and components of IWMs. The TV control algorithm with two motor in-wheel system is introduced. Instead of using a simple yaw moment control technique, A novel control technique is presented using understeer gradient characteristics

considering the dynamics of the vehicle's steady state and transient state and conducted simulation and actual test using ISO test methods for validation. In Chapter 4, another TV control algorithm with four motor in-wheel system is proposed. The control algorithm covers limit driving conditions, such as grip and slip. Side slip angle control and yaw rate control algorithm are connected in a cascaded configuration, presenting a controller with switching modes for dynamic and safety driving. To distribute the torque of the vehicle obtained from the controller to four wheels, an optimization technique with constraints is introduced to achieve optimal torque distribution. Then, the conclusion, which includes the summary and contribution of the proposed algorithm, and future works, is presented in Chapter 5.

Chapter 2 Vehicle dynamic control at limit handling

In this chapter, the dynamic characteristics of vehicle on cornering are covered, which are formulated for design torque vectoring controllers to enhance the handling performance. Vehicle and tire models are introduced for physical meaning of vehicle dynamics at limit handling. when understeer of the vehicle occurs, the human driver can solve it by reducing the speed or generating more steering in the direction to which it is originally intended. However, when oversteer occurs, it is tricky to steer the vehicle relatively properly. At this time, professional human drift technology can be a key for designing and implementing a controller, it can be applied to oversteer control in an in-wheel torque vectoring system in the future.

2.1. Vehicle Model and Analysis

2.1.1. Lateral dynamics of vehicle

There are various vehicle models to express vehicle dynamic motion, from a simple kinematic model to complicated and commercial vehicle models, which can be used in delicate vehicle dynamic analysis. For lateral dynamic of vehicle, a simplified bicycle model (2-DOF), called by a single-track model is mainly used for control design. The model was known as a yaw plane model, which also takes into account the nonlinearities between vehicle body dynamics and tire forces. In this study, designing a controller, simplified model can be easily formulated with some assumption, states of left and right wheel are identical.

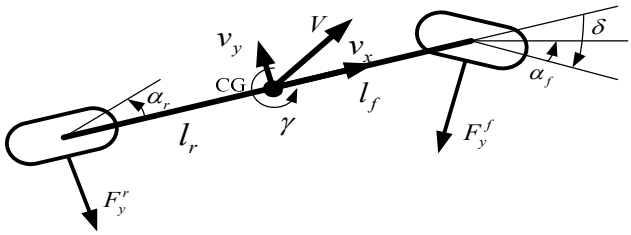

Figure 2.1. Two DOF with kinematic bicycle model

$$mv_x = F_y^f \cos\delta + F_y^r - mv_x\gamma \quad (2.1)$$

$$I_z\dot{\gamma} = l_f F_y^f \cos\delta - l_r F_y^r \quad (2.2)$$

where, F_y^f, F_y^r are front and rear lateral tire forces of the model and v_x is lateral speed, γ is yaw rate of the vehicle model. The model has two states, vehicle speed, v_x, yaw rate, γ and one control input, front steering angle, δ. The lateral tire forces are function of slip angle and slip ratio of tires, related with vehicle speed, wheel speed, and kinematic angle of tires. The slip angles α_f, α_r and slip ratio λ of tire can be expressed as

$$\alpha_f = \delta - \tan^{-1}\left(\frac{v_y + l_f\gamma}{v_x}\right) \quad (2.3)$$

$$\alpha_r = -\tan^{-1}\left(\frac{v_y - l_r\gamma}{v_x}\right) \quad (2.4)$$

$$\lambda = \frac{r\omega - v_x}{v_x} \quad (2.5)$$

where, r is the tire radius and ω is angular velocity of tire. Equation 2.3 can be induced by the kinematic relationship of steering angle and slip angle as shown in Figure 2.2.

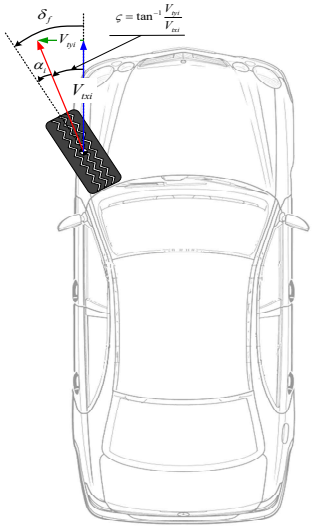

Figure 2.2 Kinematic definition of slip angle with steering angle

In following section, a controller, which can have automated steering for analyzing the limit handling condition, called drifting using the model in Figure 2.1. To express the dynamic characteristic of In-Wheel Motor system (IWMs), independent tire forces of four-wheel kinematic model also can be illustrated in planar dynamics. Therefore, this kinematic four-wheel model as shown in Figure 2.3, can be discussed in Chapter three and four. In the model, the vehicle motion parameters, side-slip angle β, and yaw rate γ can be important factors to be controlled for TV schemes in IWMs. A three degree-of-freedom yaw plane model is introduced to describe the lateral motion of vehicle that can be used by longitudinal and lateral tire forces. The kinematic equations for lateral and yaw motions using body slip angle β are similarly given by

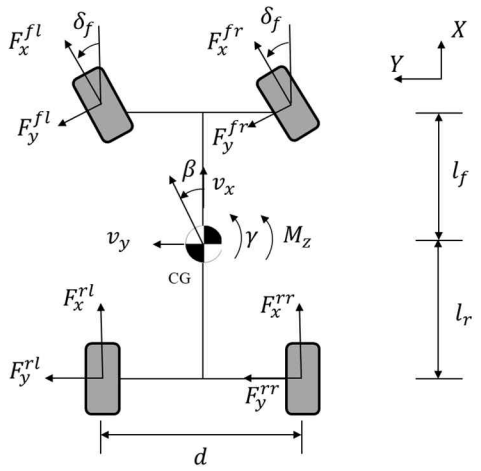

Figure 2.3 Three-of-freedom(3-DOF) Four-wheel planar model

$$mv_x(\dot{\beta}+\gamma) = F_y^f \cos\,\delta_f + F_y^r \approx F_y^f + F_y^r \tag{2.6}$$

$$I_z\dot{\gamma} = l_f F_y^f \cos\,\delta_f - l_r F_y^r M_z \approx l_f F_y^f - l_r F_y^r + M_z \tag{2.7}$$

where front lateral tire force F_y^f is the sum of the front left and right lateral fire forces (i.e., $F_y^f = F_y^f + F_y^r$). The above equations can be simplified with small angle approximation (i.e., $\delta_f \ll 1$). The yaw moment M_z is a direct yaw moment input, which is induced by the independent tire force and can be calculated as follows:

$$\begin{aligned} M_z = {} & l_f F_y^f \cos\,\delta_f - l_r F_y^r + F_x^{fl}\left(l_f \sin\,\delta_f - \frac{d}{2}\cos\,\delta_f\right) \\ & + F_x^{fr}\left(l_f \sin\,\delta_f + \frac{d}{2}\cos\,\delta_f\right) - \frac{d}{2}F_x^{rl} + \frac{d}{2}F_x^{rr} \end{aligned} \tag{2.8}$$

2.1.2. Longitudinal dynamics of vehicle

In the section, wheel dynamics and vehicle longitudinal dynamic model are

introduced to calculate longitudinal tire force F_x on the previous section. The wheel dynamic model can be shown as figure 2.4 as follows:

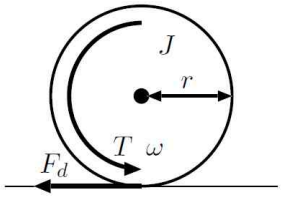

Figure 2.4 Rotational wheel dynamic model

$$J\dot{\omega} = T_i - rF_d^i \qquad (2.9)$$

where, J is the nominal wheel inertia, T_i is each wheel torque, F_d is a drag force which can be called as a traction force on tire and ground, ω is angular velocity of each wheel and tire. In the consideration of possible driving performances, it has so far been that the circumferential force acting in the tire tread area can be infinitely transferred onto the road. Indeed, according to the law of friction, the transferable traction force between the tires and road is limited by the coefficient of friction and the axle loads. This restriction results in friction induced driving limits. Besides the road and tire condition, the coefficient of friction μ, also depends on the slip between tires and road. In this case, Slip is defined the difference between wheel speed and vehicle speed relative to the reference speed.

The general form of longitudinal vehicle model as shown in Figure 2.5 can be expressed as follow:

$$m\dot{v}_x = F_d^{fr} + F_d^{fl} + F_d^{rl} + F_d^{rr} \qquad (2.10)$$

where, F_d^i is the drag force of each tire. The total longitudinal forces can be simplified by the sum of each tire drag force in Equation 2.10.

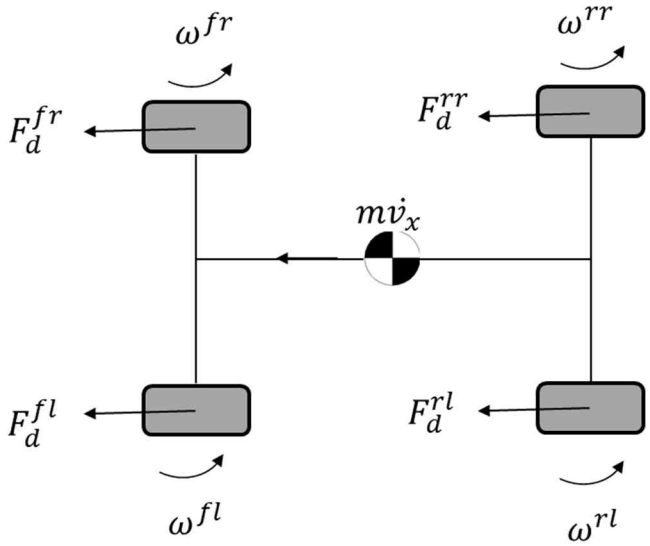

Figure 2.5 Simple longitudinal vehicle model

Figure 2.5 shows that the longitudinal forces of mass m with constant velocity $\dot{v}_x$ for a vehicle is the same as the sum of traction force of each tire. When the vehicle is accelerated or decelerated, the velocity of wheel is different to that of vehicle due to the elastic deflection of tire. Therefore, the Equation 2.5 can be defined from figure 2.6 and Equation 2.11.

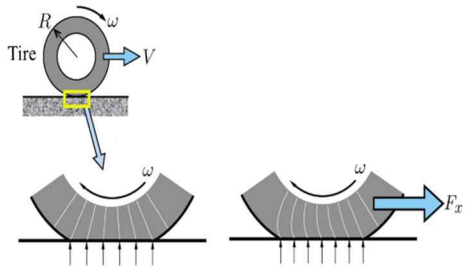

$$\lambda = \frac{V_\omega - V}{\max(V_\omega, V, \varepsilon)} \qquad (2.11)$$

Figure 2.6 Elastic deformation of tire

where, ε is a small positive number to non-zero of denominator of fraction equation 2.11. The traction force F_d^i can be related with the traction stiffness,

D_s is expressed as

$$F_d^i = \mu^i N^i \tag{2.12}$$

$$D_{s,i} = \left.\frac{dF_{d,i}}{d\lambda_i}\right|_{\lambda_i=0} \tag{2.13}$$

where, i is the index from one to four, which are each wheel of front and rear corners, μ is a road friction coefficient and N is the vertical force of wheel.

An important point to look carefully at here is the correlation between the slip ratio λ and the friction coefficient μ. The relationship can be shown in Figure 2.7 that very small area near the origin of slip ratio is linearly proportional to the friction coefficient but other area of that is that as the slip ratio increases, the friction coefficient decreases. In addition, the slope of the linear section has a steep slope on a high friction road surface and a gentle slope on a low friction road surface. When the inclination decreases in this way, the maximum coefficient of friction between the wheel and the road surface decreases, resulting in a situation in which sufficient frictional force cannot be obtained. As a result, whether on a high or low friction road, we need to control the amount of wheel slip to be within a linearly increasing area.

In general, the maximum coefficient of adhesion friction is reached when the slip ratio is 10-20%. As the slip increases, the coefficient of friction gradually decreases and becomes the coefficient of sliding friction at 100% slip. The variation of tire forces according to the slip ratio and slip angle will be dealt with more details on the following section.

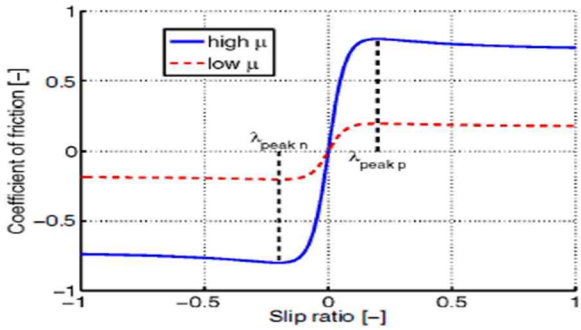

Figure 2.7 Characteristics of slip ratio

2.2. Tire Model

The characteristics of vehicle tires are composed of pneumatic components, rubber, and other iron materials, which are components of the tire, and have very high nonlinearity and are greatly affected by the surrounding environment. Therefore, it is also quite difficult to construct a dynamic model considering the physical characteristics of the tire.

The tire model is simply used in the controller design using a linear relationship, and the model's inaccuracy can be considered as the controller's uncertainty. However, in this study, more detailed tire models are introduced for designing in-wheel motor control in the future by analyzing the relationship between the fun to drive and stability of the vehicle through control in the limit situation of the vehicle and tire.

In general, the Fiala tire model based on the theory of basic tire dynamic and based on empirical formula, the Pacejka and Bakker tire model, which is the most widely used in commercially, are considered. While the Fiala tire model expresses the force of a tire using a brush model with physical valued

parameters, the Pacejka and Bakker tire model does not much have physical meanings, and the parameters are obtained through curve fitting using the data obtained in the experiment.[Goh and Gerdes 2016]

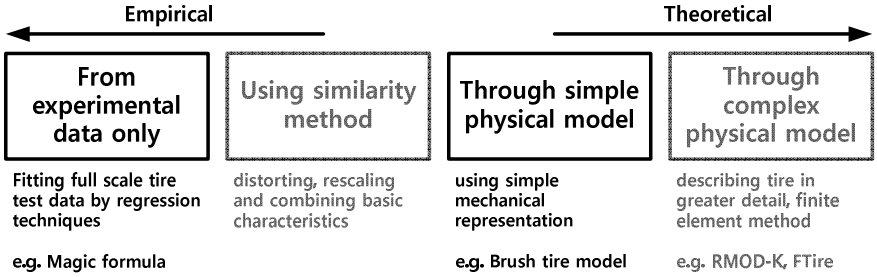

Figure 2.8 Classification of tire models

At first, to use lateral tire forces to be used in the vehicle lateral dynamic model, the Fiala tire model can estimate lateral tire forces F_y^f and F_y^r with inputs and parameters to the tire model. The front and rear slip angles of tires α_f, α_r are the inputs to the tire model; all other terms are treated as constant parameters. The Fiala model is given be the following non-linear piecewise function,

$$F_y(\alpha) = \begin{cases} -C_\alpha \tan\alpha - \dfrac{C_\alpha^3\left(1-\dfrac{2\mu_s}{3\mu_p}\right)}{9\mu_p^2 F_z^2}\tan^3\alpha \\ + \dfrac{C_\alpha^2\left(2-\dfrac{\mu_s}{\mu_p}\right)}{3\mu_p F_z}|\tan\alpha|\tan\alpha & : |\alpha| < \alpha_{s1} \\ -\mu_s F_z \, sgn\ \alpha & : |\alpha| \geq \alpha_{s1} \end{cases} \quad (2.14)$$

where, α_f , α_r = *Slip angle of Front/rear tire*

C_α = Tire *cornering stiffness*

μ_s = *Sliding friction coefficient*

μ_p = *peak friction coefficient*

F_z = *Normal load applied to the tire*

$$\alpha_{s1} = \tan^{-1}\frac{3\mu_p F_z}{C_\alpha}$$

The Fiala tire model can be used in the next section for tire inverse model and finding the equilibrium points which will be regulated by drift control.

The Pacejka and Bakker tire model is based on a curve for which the parameters have no physical meaning; measurement data is used to fit the parameters best to the collected data. The lateral tire forces with lateral slip angle, can be introduced firstly for simplicity of model. As shown in Figure 2.9, the lateral tire force can be expressed as a nonlinear concave function. The lateral force increases as slip angle increases below peak slip angle and if slip angle exceeds peak slip angle, lateral force does not increase.

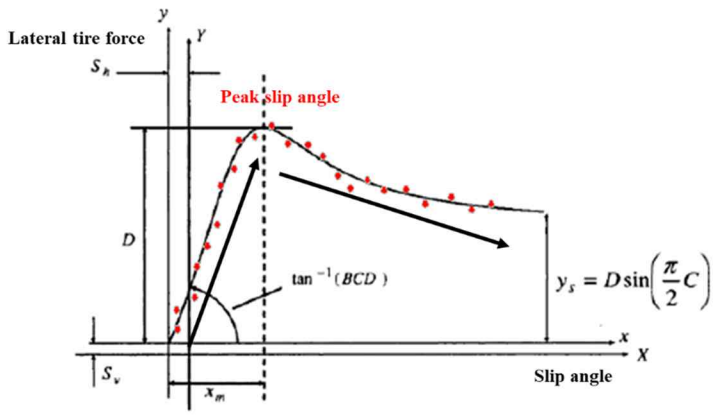

Figure 2.9 lateral tire forces with pure slip angle

The Pacejka and Bakker tire model is applied in this study. Longitudinal and lateral tire forces are determined by slip ratios and slip angles, respectively. The longitudinal tire force is obtained by the magic formula as follows.

$$F_x = D_x \sin[C_x \tan^{-1}(B_x \Phi_x)] + S_{vx}$$
$$\Phi_x = (1 - E_x)(\lambda + S_{hx}) + \frac{E_x}{B_x}\tan^{-1}(B_x(\lambda + S_{hx})) \quad (2.15)$$

where, D_x is scaling factor, C_x is shape factor, and B_x is stiffness factor. The factors determine the shape of the magic formula curve with respect to slip ratio.

The lateral tire force is obtained by the magic formula as a function of slip angle.

$$F_y = D_y \sin\left[C_y \tan^{-1}(B_y \Phi_y)\right] + S_{vy}$$
$$\Phi_y = (1 - E_x)(\alpha + S_{hy}) + \frac{E_y}{B_y} \tan^{-1}(B_y(\alpha + S_{hy})) \quad (2.16)$$

where, D_y is scaling factor, C_y is shape factor, and B_y is stiffness factor. The factors determine the shape of the magic formula curve with respect to slip angle. Therefore, tire force with combined slip, which has longitudinal slip ratio and lateral slip angle, can be calculated by vectoring resultant force as shown in Fig 2.10. The lateral force increases as slip angle increases below peak slip angle while slip angle exceeds peak slip angle the lateral forces does not increase as shown in Figure 2.10. Considering the constant lateral force such as red line on Figure 2.10, the more slip ratio increase, the more slip angles are needed for same lateral force.

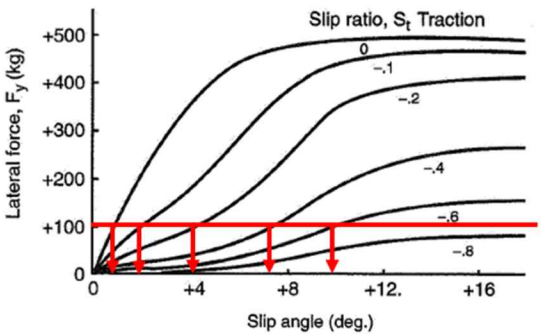

Figure 2.10 Tire lateral force with combined slip ratio and slip angle.

In this model, there are numerous parameters and various conditions to be

calculated as various factors which can be affected by tire-road friction coefficients, road roughness, temperature, pressure of tire, tire wear and so on.

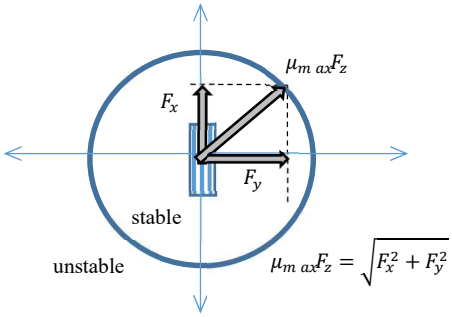

Figure 2.11 Kamm's friction circle principle

Considering the characteristics of Combined tire forces, tire forces can be simplified with relationship between slip angle and slip ratio. Friction circle principle can be introduced for transferable forces from the tire to the road surface by Wunibald Kamm, who has been worked at Daimler and founded the Research Institute of Automotive Engineering at Technical University of Stuttgart in the 1930's. As shown in Figure 2.11, the magnitude of the total frictional force does not exceed the sum vector magnitude of the lateral and longitudinal forces. Using the principle, the relationship with tire forces can be explained in torque vectoring control system.

2.3. Analysis of vehicle drift for fun-to-drive

In this section, among the limiting driving conditions of the vehicle, the progress was focused on the advance development of a control technique that enables the driver to fun to drive while simultaneously improving stability and drivability in the turning limit. Analysis in such limiting driving can also be of

great help in torque vectoring control. In particular, by developing an autonomous drift controller for drift driving conditions in high-speed turning limit situations, we intend to contribute to the future drift support or the stability of the in-wheel torque vectoring system.

Main skill of human drift technology, which is generally known, seems to be able to be defined as Steady-state cornering and precise adjustment in situations where the friction limit of the rear tire is exceeded. In addition, it has three main characteristics when it is classified based on this drift phenomenon. First, the vehicle traveling direction and the vehicle heading direction must be different and have a large body slip angle, β. The second has steering in the opposite direction to the direction the vehicle turns (counter-steer). The last characteristic is that wheel spin should be generated due to the large driving torque of the rear tire for yaw moments. This drifting run is often used in rally competitions under conditions where the friction coefficient of the road surface is unknown or changing. Unlike normal cornering, the slip angle of the vehicle near the friction limit of the rear tire, which is the drift characteristic, is no longer a small value. It appears almost in the order of several dozen degrees (deg). Currently, it can be seen that the slip angle of the rear wheel and the slip angle of the vehicle are decoupling with the moving direction of the CG from the heading of the vehicle.

Since drifting can define a steady state cornering with saturated rear tires, it is necessary to analyze the equilibrium of a vehicle with a saturated rear tire. This

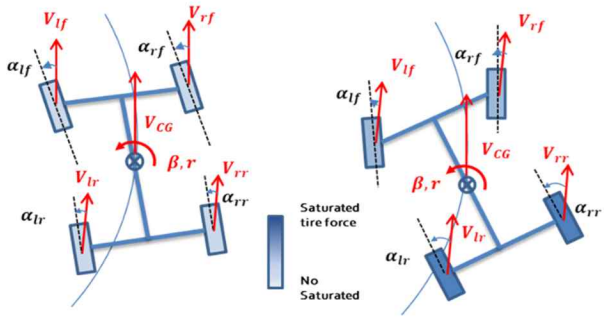

Figure 2.12 Normal grip cornering and drift cornering

is also used in several papers, and an open-loop unstable drift equilibrium was derived using a simple bicycle model with non-linear tire model[xxx]. The vehicle's slip angle and yaw rate trajectory were expressed using phase portrait analysis.

It can be considered to perform drift in the normal circle turning condition of a vehicle with saturated rear tires for equilibrium analysis. A general nonlinear system is x =$\boldsymbol{f}$ (x, u), where x is a state vector and u is an input vector. Therefore, the equilibrium point of the system occurs at each equilibrium state, x_{eq}, and the input corresponding to the value, u_{eq}, and occurs at the point where the derivative of the state variable is *0*.

$$f(\mathbf{x}^{eq}, \mathbf{u}^{eq}) = 0 \tag{2.17}$$

Using side slip angle(β) can be defined as $\beta = \tan^{-1} v_y / v_x$ and Equation 2.1 and 2.2, side slip angle and yaw rate equations are below:

$$\dot{\beta} = \frac{F_{yf}\cos\delta + F_{yr}}{mv_x} - \gamma \tag{2.18}$$

$$\dot{\gamma} = \frac{l_f F_{yf} \cos\delta - l_r F_{yr}}{I_{zz}} \quad (2.19)$$

Using equation 2.18, 2.19 and steady-state cornering condition ($\dot{v}_x = \dot{v}_y = \dot{\gamma} = 0$), the equilibrium points can be found as

$$\frac{F_{yf}^{eq} \cos\delta + F_{yr}^{eq}}{m v_x^{eq}} - \gamma^{eq} = 0 \quad (2.20)$$

$$\frac{l_f F_{yf}^{eq} \cos\delta - l_r F_{yr}^{eq}}{I_{zz}} = 0 \quad (2.21)$$

$$F_{yr}^{eq} = F_{yr,0}^{eq} \cdot \frac{\sqrt{(\mu F_z)^2 - (F_{xr})^2}}{\mu F_z} \quad (2.22)$$

where, $F_{yf}^{eq}, F_{yr}^{eq}, \beta^{eq}, \gamma^{eq}, v_x^{eq}$ are the lateral forces, side slip angle, yaw rate, and driving speed of an equilibrium point. Equation 2.22 shows that the original lateral force, $F_{yr,0}^{eq}$ can be considered as the fraction of de-rated ratio by rear traction force. In order to solve Equation 2.20 and 2.21, the lateral forces, a non-linear function of slip angle with non-linear tire model cannot be found as an explicit solution but solved by numerical method with MATLAB.

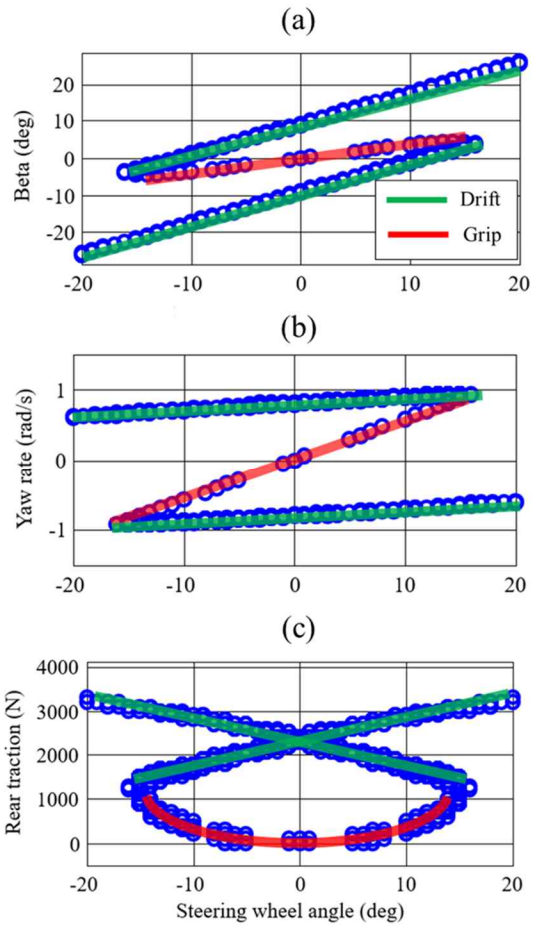

Figure 2.13 Equilibria of drift and grip with bicycle model

Figure 2.13 shows that the equilibrium sideslip, yaw rate, and rear lateral force as a function of the equilibrium steering wheel angle. Note that the system has multiple equilibrium conditions for several of the steering wheel angle considered. Using Equation 2.20 and 2.21, nonlinear and multiple solution can be calculated by algebraic equations. Close study of these plots reveals that the model has two groups of equilibria, indicated in the figures by green and red

lines. A red line in Figure 2.13 (b) shows the linear relationship between the steering angle and yaw rate, with yawing more in steady-state as the steering angle is incleased. The preceeding figures do not provide any information about the stabilityof equilibia, or the dynamic chracteristics of the model around the equilibria. Figure 2.14 is the phase portrait plots which can examinate the dynamic stable status and characteristics.

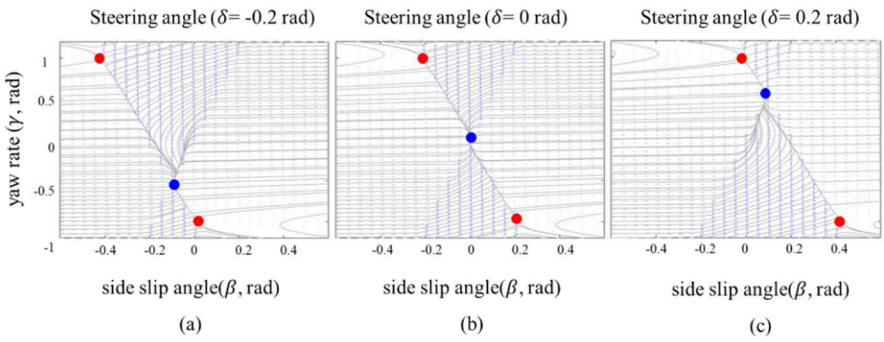

Figure 2.14 Phase portrait of state trajectories at $v_x^{eq} = 10m/s$.

Phase portrait plots are generated by simulation with a model for a variety of initial conditions in the state space. For the fixed steering angles, $\delta = \delta^{eq}$ and constant speed, $v_x = v_x^{eq}$, the bicycle model can be simulated. Figure 2.14 (a), (b) and (c) are plotted using simulation with $v_x = 10m/s$ and $\delta = 0, 0.2,$ and *-0.2 rad*. The equilibrium locations in each plot are denoted by red and blue dots. The number of three equilibrium points in Figure 2.13 is equal to that of equilibrium points in Figure 2.14, and two instability points and one stability point are recognized. The blue dots in Figure 2.14 are the stable equilibrium coreespondes to normal cornering underneath tire saturation. The remaining red dots in the same figure are regarded as drift driving equilibria with considerable side slip angle. Another notable point here is the observation that the red dots,

not close with blue dots in Figure 2.14 (a) and (c), are located at different signed yaw rate amplitude with the sign of steering angle. It means that the cornering direction in drift cornering is opposite of steering wheel angle, those are typical drift driving with expert driver, to balance the front and rear tire forces for keeping drift behavior. Therefore, a close observation of the phase portrait indicates that the physical meaning around the equilbria in terms of vehicle dynamics can be examinated qualitatively. Finally, the unstable equilbria can be regulated using sliding mode control technique for limit cornering conditions.

2.4. Designing A Controller for Automated Drift

In previous section, stable or unstable equilibria points has been analyzed with physical meanings. Therefore, this section seeks to address controller design for actual simulation and practical application using conditions of drift situations obtained from previously induced and modeled vehicle models, and equilibrium point analysis. The design of the controller can be coordinated using multiple control techniques, depending on input and output, or depending on whether the system to be controlled is linear or nonlinear. In this study, a vehicle system performing a drift to be controlled is a condition to use a controller with the following characteristics:

- Fast output response with control input
- Low computational effort
- Be robust in the disturbance that affects the state
- Control using non-linear system models

Therefore, the above-mentioned conditions are satisfied, and the sliding mode control can be implemented with high application range in the future.

For control of nonlinear systems, the main area of interest is to apply control

theory to micro-processors through the discretization of signals, and to discretize these continuous-time systems so that they can be stabilized by supplementing the process of external and unstable discretization.

Sliding mode control techniques are one of the toughness control techniques that show robust and invariant performance against uncertainty or disturbance of the model under control. To achieve this advantage, we design a pre-stable sliding surface in the state space and use the switching input signals to ensure that the state of the system converges from the state space to the sliding plane and does not deviate from it. Typically, this sliding mode control uses a switching function, so it is inevitable that chattering takes place near the surface being sliding, which can pose a major problem in real-world applications. Therefore, many studies are being conducted to eliminate this chattering phenomenon, in which we discretize continuously changing functions to set the sliding surface and implement stable control. In this work, we set the sliding surface by discretizing continuously changing functions and proceed to implement stable control.

2.4.1. Lateral controller

In Equation 2.20 and 2.21, the state vector $\mathbf{x} = [\beta \quad \gamma]^T$ for a fixed parameter v_x and the input vector $\mathbf{u} = [F_{yf} \quad F_{yr}]$ for control inputs can be considered. Using the inverse tire model, F_{yf} can be controlled by steering angle on front and F_{yr} by engine torque.

Firstly, the sliding surface can be defined as

$$s_1 \triangleq \beta - \beta^{eq}, \qquad s_2 \triangleq \gamma - \gamma^{eq} \tag{2.23}$$

where, β^{eq} and γ^{eq} are constants, Equation 2.23 can be differentiated as

$$\dot{s_1} \triangleq \dot{\beta}, \qquad \dot{s_2} \triangleq \dot{\gamma} \tag{2.24}$$

Using Equation 2.18, 2.19 and Euler approximation to discretize the dynamics:

$$s_1(i+1) \approx s_1(i) + T_s\dot{\beta}, \qquad s_2(i+1) \approx s_2(i) + T_s\dot{\gamma} \tag{2.25}$$

where, T_s is sampling time of system discretization. Therefore, using Equation 2.25, the slip angle and yaw rate equations can be expressed as

$$\begin{aligned} \dot{\beta}(i) &= \frac{\left(F_{yf}(i) + F_{yr}(i)\right)}{mv_x} - \gamma(i), \\ \dot{\gamma}(i) &= \frac{l_f F_{yf}(i) - l_r F_{yr}(i)}{I_{zz}} \end{aligned} \tag{2.26}$$

Next, for designing the sliding control mode, a function for reaching law to the surfaces has to be defined. This function can be expressed as follows by discretizing the solution of the first differential equation.

$$s_1(i+1) \triangleq \rho_1 s_1(i), \quad s_2(i+1) \triangleq \rho_2 s_2(i), \quad 0 \le \rho_{1,2} < 1 \tag{2.27}$$

Equation 2.27 can be put into Equation 2.25 and Equation 2.26 can be simplified as

$$K_1(i) = mv_x\left[\gamma(i) + \frac{(\rho_1 - 1)}{T_s}(\beta(i) - \beta^{eq})\right] \tag{2.28}$$

$$K_2(i) = \left[\frac{I_{zz}}{T_s}(\rho_2 - 1)(\gamma(i) - \gamma^{eq})\right] \tag{2.29}$$

where,

$$K_1(i) \triangleq F_{yf}(i) + F_{yr}(i), \quad K_2(i) \triangleq l_f F_{yf}(i) - l_r F_{yr}(i) \tag{2.30}$$

In order to find the forces F_{yf} and F_{yr}, Equations 2.28 and 2.29 can be rearranged as

$$F_{yf}(i) = K_1(i) + \frac{K_2(i) - l_f K_1(i)}{l_f + l_r} \tag{2.31}$$

$$F_{yr}(i) = \frac{l_f K_1(i) - K_2(i)}{l_f + l_r} \quad (2.32)$$

Equation 2.31 and 2.32 can be analyzed with physical meaning that the control inputs are obtained by inputting the lateral tire forces to slide the vehicle into drifting. Therefore, the real vehicle input, the steering angle which can be calculated by Equation 2.31 and 2.32, can be used for simulation and test. Suppose the front tire is not saturated and slipped on longitudinal direction, the front steering angle can be simply found as

$$\delta_f(i) = \beta(i) + \frac{L_f \gamma(i)}{v_x} - \alpha_f(i) \quad (2.33)$$

where, α_f is the front tire slip angle.

The front tire force which is a function of tire slip angle α_f, can be found using the inverse tire models (ITM).

2.4.2. Longitudinal Controller

The lateral force of a steering controller is actually a part with non-linear properties, depending on the forces and conditions in other directions applied to the tire. Assuming a reasonable level of assumption, the model is inaccurate, but the use of a robust controller is sufficiently overcome, so it can be seen that using sliding control is significant in practical applications. In addition, there shall be a rear tire saturation which is the basic condition of drift control. As $F_{yf}(i)$ is used to determine the required steering angle and obtained from the invert tire model (ITM), $F_{yr}(i)$ is available as a boundary condition for the saturation of the rear tire. Using equation 2.5 and 2.9, the slip ratio λ can be calculated as

$$\lambda = \frac{r_e\omega_e - v_x}{r_e\omega_e} \quad (2.34)$$

where, r_e is the effective rolling radius and ω_e is the angular velocity of tire. The constraint of the tire forces of vehicle can be simply expressed using Kamm's friction circle principle as below:

$$F_{xr}^2 + F_{yr}^2 \leq \mu F_{zr}^2 \quad (2.35)$$

Based on the above the equation, F_{xr} can be calculated and found using ITM for longitudinal slip ratio λ which can be controlled by the traction and braking forces of the vehicle. Therefore, the third sliding surface using wheel dynamics, can be defined as

$$s_3 = (r_e\omega_e - U_x) - (r_e\omega_e^d - v_x^d) \quad (2.36)$$

where, ω_e^d is a desired angular velocity of wheel and v_x^d is a desired longitudinal vehicle speed.

The second term of Equation 2.36, $r_e\omega_e^d - v_x^d$ can be assumed as a constant term and the final differentiated sliding surface $\dot{s}_3$ can be expressed as

$$\dot{s}_3 = r_e\dot{\omega}_e - \dot{v}_x\,, \qquad I_w\dot{\omega}_e = T_w - r_eF_{xr} \quad (2.37)$$

where, T_w is the traction and braking torque of wheel.

Similar method in previous section, discretization and a tuning parameter can be applied to find a reaching law,

$$s_3(i+1) = \rho_3 s_3(i), \qquad 0 \leq \rho_3 < 1 \quad (2.38)$$

Therefore, the longitudinal wheel torque can be calculated as

$$T_w(i) = r_eF_{xr}(i) + \frac{I_w}{T_s r_e}[(\rho_3 - 1)s_3(i) + \dot{v}_x(i)T_s] \quad (2.39)$$

Designing the sliding controller of discretization has been applied, and the sliding surfaces consisted of three types, and the key formulas of steering control and drive control were induced and applicable.

2.4.3. Stability Analysis

A general scalar nonlinear state equation in continuous time domain can be stated as below:

$$\dot{x}(t) = f(x,t) + g(x,t)u(t) \quad (2.40)$$

With a first order Euler discretization using sampling time T_s, Equation 2.40 can be rewritten as

$$\dot{x}(t) \approx \frac{x(i+1) - x(i)}{T_s} \quad (2.41)$$

$$x(i+1) = x(i) + [f(x,t) + g(x,t)u(t)]T_s \quad (2.42)$$

A sliding surface can be defined as the difference between the desired state and actual state as Equation 2.43.

$$s(i) \triangleq x(i) - x_d(i), \qquad s(i+1) = x(i+1) - x_d(i+1) \quad (2.43)$$

In the previous subsection, a parameter ρ has been defined for reaching law that the sliding surface will be zero. Generally, in sliding mode control, the reaching law to sliding surface in continuous time uses signum function which may cause chattering vibration. However, if the parameter ρ would be continuously changes into small value, the controller can be reduced the chattering effects. Therefore, the reaching law in Equation 2.27 can be expressed as

$$s(i+1) \leq \rho|s(i)|, \qquad 0 \leq \rho < 1 \quad (2.44)$$

Using the discrete Lyapunov function and its difference equation are shown and detailed as follow [Edelberg, Pan, and Hedrick 2013]

$$V(i) = \frac{1}{2}s(i)^2 > 0 \quad (2.45)$$

$$\triangle V(i) = V(i+1) - V(i) = \frac{1}{2}s(i+1)^2 - \frac{1}{2}s(i)^2 \qquad (2.46)$$

From Equation 2.44 and 2.46, the negative definite can be induced for asymptotical stable state vectors, the equation can be rewritten as

$$\begin{aligned} \triangle V(i) &= \frac{1}{2}(\rho^2 - 1)s(i)^2 \\ &= \frac{1}{2}(\rho^2 - 1)\big(x(i) - x_d(i)\big)^2 < 0 \end{aligned} \qquad (2.47)$$

The state $x(i)$ is can be the yaw rate or slip angle which is a positive definite function.

2.4.4. Validation with simulation and test

A. Simulation

Using the designed sliding mode controller in the previous subsection, several simulation study and test validation can be done with CarSim and Matlab/Simulink, commercial software for vehicle dynamic and control. Figure 2.15 illustrates the setup of simulation with equilibrium points. The vehicle parameters and simulation conditions can be found in Table 2.1.

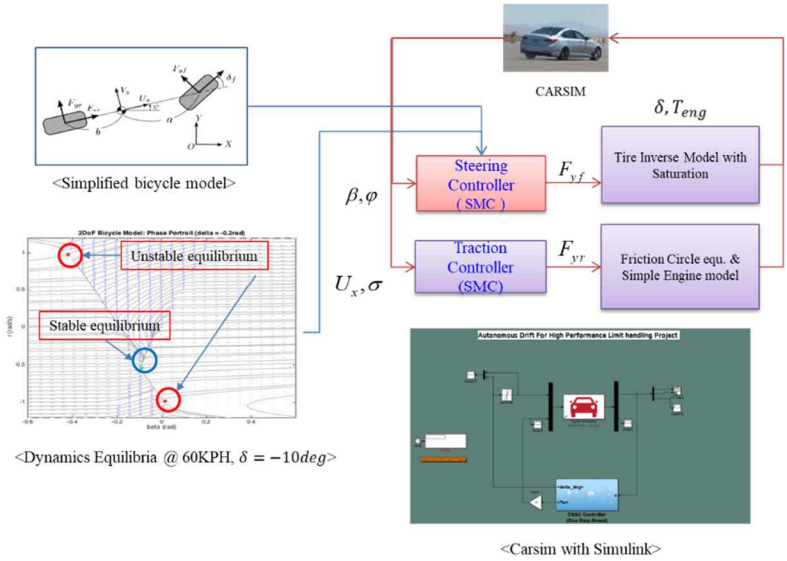

Figure 2.15 The schematic of drift simulation setup

Symbol	Parameter	Value
m	Total vehicle mass	1800 kg
l_f	CG-front axle distance	1.402 m
l_r	CG-rear axle distance	1.598 m
C_f	Tire cornering stiffness of front axle	120,000 N/rad
C_r	Tire cornering stiffness of rear axle	120,000 N/rad
L	Wheelbase	2.836 m
I_z	Yaw moment of inertia	2800 kgm^2

Table 2.1 Vehicle parameters for simulation

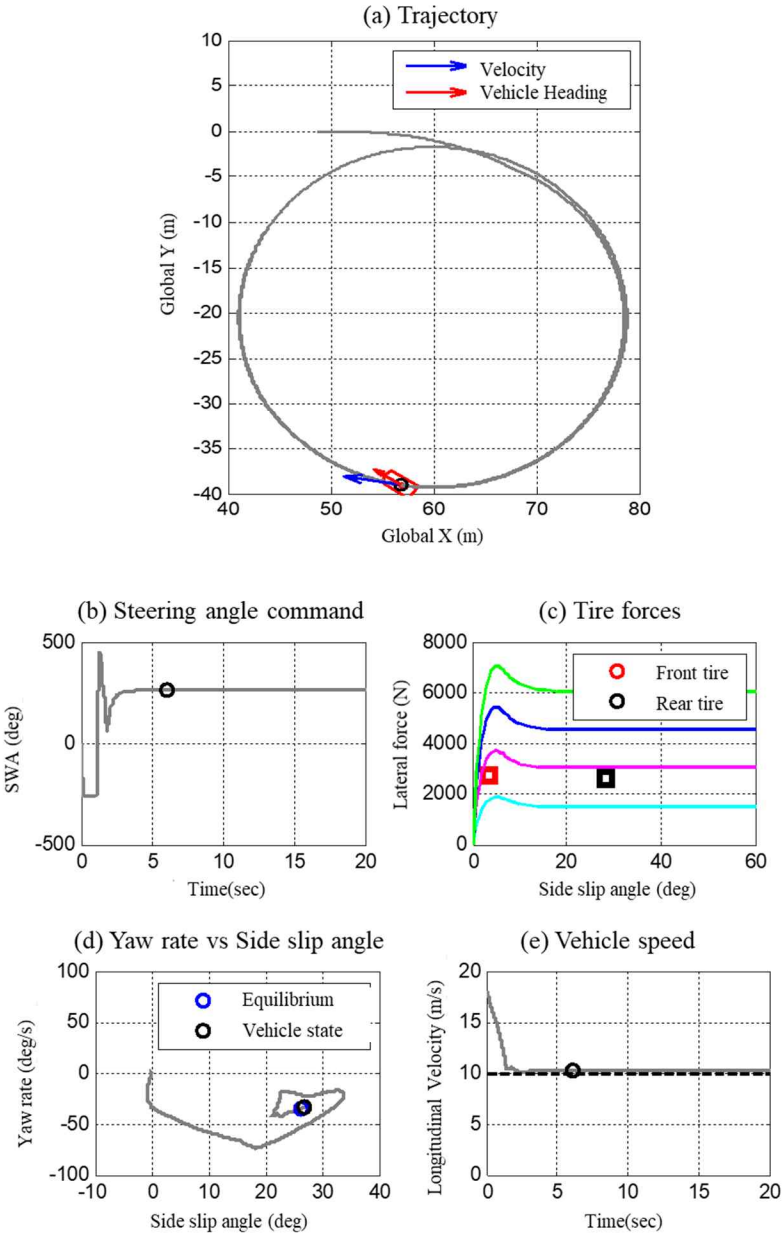

Figure 2.16 Simulation results with equilibrium points

The simulation study, which has an equilibrium point with the parameters,

$\delta_f^{eq} = 20deg$, $v_y^{eq} = \frac{4.29m}{s}, \gamma^{eq} = -\frac{0.6rad}{s}, v_x^{eq} = \frac{10m}{s}, F_{xr}^{eq} = 3250N$ can be plotted in Figure 2.16. Tracking the Equilibrium point, already found on offline, the yaw rate and sideslip angle, has good performance as shown in Figure 2.16 (c). In Equation 2.23, tuning parameters, ρ_1 and ρ_2, serve to change the rate of convergence and the importance of convergence in reaching the equilibrium point of the states. Even the non-linear dynamics in this system has highly governed, the automated drift can be stably controlled by the developed discrete sliding mode controller.

B. Real car Test

In Figure 2.17 shows the experimental set-up, such as experimental vehicle, DGPS, Micro-Autobox, battery system and data acquisition system. The DGPS from Oxford Technical Solution is a high-precision differential GPS system, so that the sideslip angle and yaw rate measured by RT3002 is regarded as an actual value. This device is located close CG of the vehicle. The control inputs are active steering angle with MDPS (Motor Driven Power Steering) and engine torque for making rear tire force. The inputs can be controlled using CAN messages. The numbers of tunning parameters for the experimental vehicle are presented in table 2.2. The vehicle as shown in Figure 2.17 is a Hyundai Luxury sedan, which has 5.0L gasoline engine with rear wheel driven drivetrain. Rear differential has an electric Limited Slip Differential (eLSD) which can limit torques of left and right-side wheels. This system can help jumping to the drift condition because the rear outside wheel torque does not transfer to inside wheel. It means that eLSD can limitedly control the torque between left and right wheel.

Figure 2.17 Test vehicle and equipment.

Symbol	Parameter	Value
β_{eq}		25 deg
γ_{eq}		30 deg/s
v_{xd}		50 km/h
ρ_1		0.82
ρ_2		0.19
ρ_3		0.6

Table 2.2 Tunning parameters of Automated drift controller

Figure 2.18 shows several plots of the results of an experiment on a real vehicle. Compared to the simulation results as shown in Figure 2.16, the actual experiments result in the fluctuation in the plots of vehicle speed, yaw rate, and.

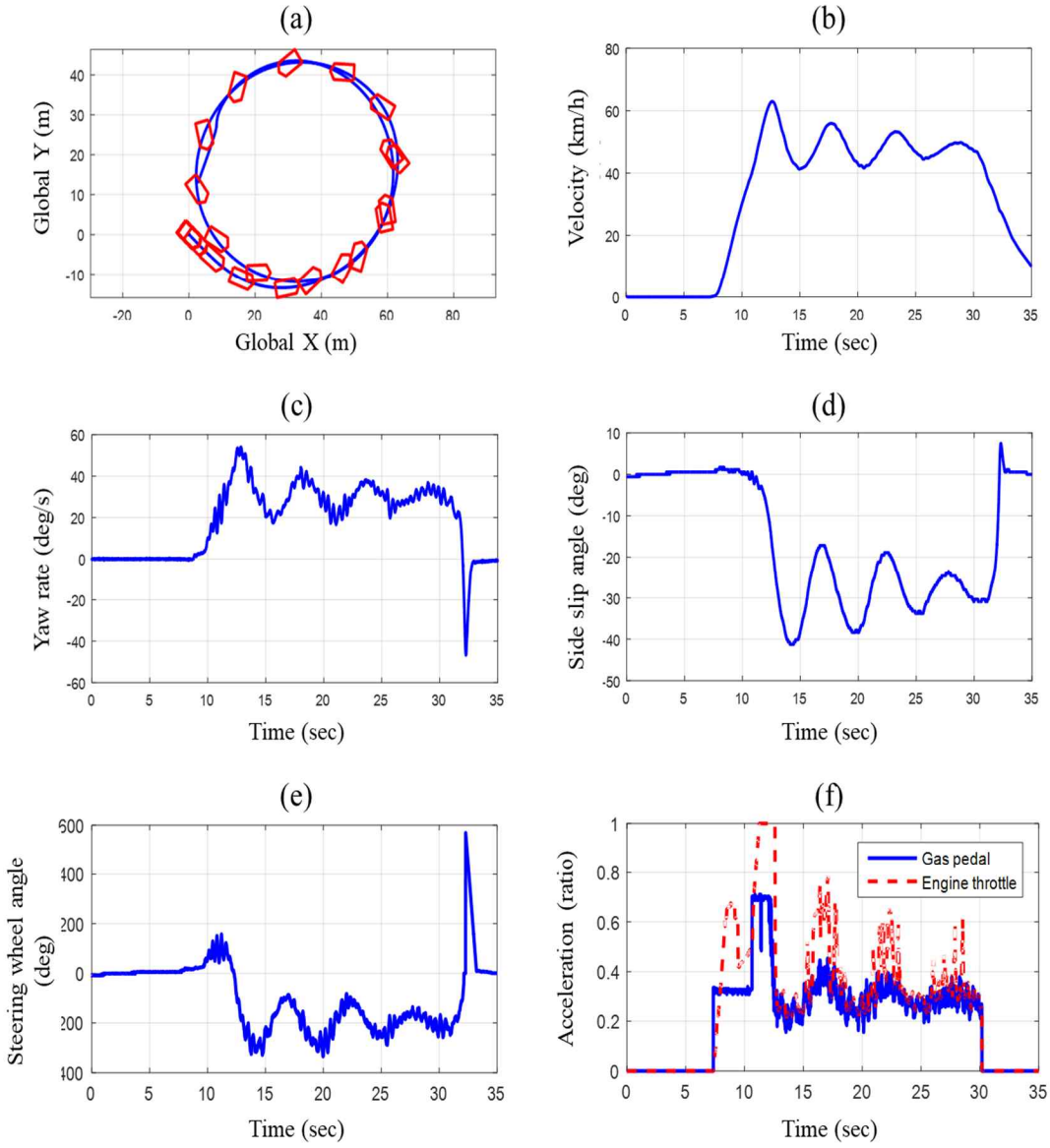

Figure 2.18 Vehicle test results

side slip angle, resulting in some differences from the simulation results. It can be considered that the fluctuations are caused by nonlinearity of tire and traction control between the grip and slip regions of tires and the inertia of the acceleration of the internal combustion engine

However, the target yaw rate and side slip angle can be controlled as shown in Figure 2.18, tracking those values on average. In the case of drift-specialized drivers, when a general vehicle is used, it is driven in a circle with fluctuations. Therefore, automated drift controllers also exhibit good performance.

Chapter 3 Torque Vectoring Control with Front Two Motor In-Wheel Vehicles

In the previous chapter, the vehicle's dynamic characteristics are described in the vehicle's limit handling situation, which can be based on the performance of torque vectoring control, and in the resulting turning limit area. In particular, automated drift control has been able to be controlled beyond the friction limits of the rear wheels of the vehicle, which, as described in Chapter 2, showed the possibility of an assist function that enables fun to drive during torque vectoring. It is possible to configure a support mode that only experienced drivers can experience by applying drift technology that only experienced drivers can experience it.

In this chapter, using the dynamics of the vehicle at limit driving condition analyzed in Chapter 2, the application of the in-wheel system of electric vehicles and the application of torque vectoring control techniques are covered. First, we introduce torque vectoring control techniques for two motor in-wheel systems and perform verification through simulations and real vehicle experiments.

3.1. Dynamic Torque Vectoring Control

3.1.1. In-wheel motor system (IWMs)

Motor driven electric vehicle system provides additional capability to vehicle while conventional vehicle, controlled by steering and gas/brake pedal, in-wheel motor vehicle can control longitudinal, lateral and vertical forces on four palm size tire contact [Joa et al. 2020].

The basic idea of torque vectoring is that given requests from the driver (steering angle, brake, and acceleration with pedal signals) will be processed and distributed as torque commands to the wheels of the vehicle. With the individual torque distribution, the vehicle handling performance, fun-to-drive (agility) and safety can be improved [Kaiser et al. 2011]. In this section, the torque vectoring control with two in-wheel motor system can be considered as a target plant system for safety and fun to drive purposes.

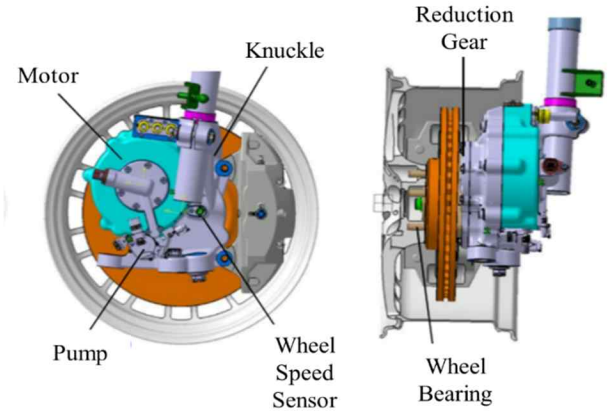

Figure 3.1 Schematic of In-wheel Motor system [Mobis 2016]

Figure 3.1 is the schematic of In-Wheel Motor system (IWMs) for a proto-type product. IWMs is modified on conventional knuckle which can mount a wheel

and tire assembly with braking system. The IWMs consists of motor, reduction gear, and oil circulation system in modified knuckle system which exists in the wheel. The IWMs, compared with a conventional powertrain with transmission and driveshaft, is directly connected from electric power system to wheel and tire system. The IWMs are placed under the spring, which has the following advantages: The motor is more responsive than the internal combustion engine with good response to friction brakes by hydraulic control. The generated torque can be accurately determined by the current value. Positive and negative rotation torque may be generated. The inertia moment of the driveshaft and spring is controlled below the torsional natural frequency, but IWMs can be controlled with high responsiveness even at high frequencies. Compared to the case of the driveshaft, the upper and lower torsion of the driveshaft is large, so it can be used to improve the ride. Especially, the IWMs on four wheels, in all vehicle motion performances, such as driving, turning, braking, and ride comfort, which are characteristics of the car, has various and excellent functions. Compared to brake control on conventional system, the range of operation can be extended to the linear area of the tire, replacing the vehicle motor control actuator other than steering, and performing better.

3.1.2. Dynamic system modeling

In this study, a commercial passenger car with IWMs will be considered as a plant to be controlled. Torque vectoring control is very deep relationship with steer characteristics, which is understeer or oversteer during vehicle cornering. Understeer and oversteer are vehicle dynamics terms used to describe the sensitivity of a vehicle to steering. Oversteer is what occurs when a car turns by more than the amount commanded by the driver. Conversely, understeer is

what occurs when a car steers less than the amount commanded by the driver[International Organization for Standardization 2010]. Most modern passenger cars are setting to get understeering behavior when it is driven on corner of road for safety reasons with kinematic and compliance characteristics of conventional suspension and steering system.

There are usually measured as slopes of the response curves at 0.1g in the linear range of tire performance. General Motors Proving Ground, for example, uses the Constant Circular Test(CCT) and for passenger cars has standardized on a test speed of 100 km/h summarizes the results of measurement on 169 cars[Milliken 1994]. Recent research from Hyundai Motors Proving Ground also uses the constant radius test with similar way with 50 modern cars (’90 ~). The average results are given in Table 3.2 and 3.2. When compared to the passenger car, sports cars have less understeer gradients.

Understeer Gradient(deg/g)	Minimum	Average	Maximum
Passenger car	0.7	4.4	8.2
Sport car	1.17	2.01	5.53

Table 3.1 US gradient test with 169 cars, CCT by General Motors

Understeer Gradient(deg/g)	Minimum	Average	Maximum
Seg. A/B car	1.8	2.05	2.42
Seg C/D car	1.5	1.8	2.3
Seg SUV car	2.10	2.33	2.8
Sport / HPV car	1.09	1.25	1.54

Table 3.2 US gradient test with 59 cars, CCT by Hyundai motors

Those results were gathered in a condition of steady-state response, which means stable cornering of those vehicles such as a time invariant system. However, in real driving condition, steady-state and transient conditions coexist, and when the vehicle is driven in a cornering, it appears in a combined state. For this reason, the name of following control system is expressed as a dynamic torque vectoring control.

Most of researches [Park et al. 2020, Canale et al. 2008, Yang, Idegren, and Jonasson 2018, Kaiser et al. 2011] employed steady-state response with appropriate delay to design target yaw rate. However, steady-state response deviates from actual vehicle response and delay can be varied with vehicle states. In real vehicle, the direction of motion of the ends of the vehicle also depends on such items bump steer, roll steer, camber, lateral & longitudinal load transfer and compliance steer from the road forces. Theses may be accommodated by working out or measuring " effective slip angle steers" and their difference($\alpha_f - \alpha_r$) [Milliken 1994]. From the cornering kinematics of the bicycle model, the required steering angle can be written as [Milliken 1994]

$$\delta = \frac{L}{R} + \alpha_f - \alpha_r = \frac{L}{R} + \frac{F_{yf}}{C_f} - \frac{F_{yr}}{C_r}, \quad (3.1)$$

where, δ is the wheel angle for steering, L is the wheelbase, R is the road curvature, α_i is the slip angle of each tire, F_{yi} is the lateral force of each tire, and C_i is the cornering stiffness of each tire. With steady-state assumption, the difference between the front and rear slip angles in Equation 3.13.13.1 can be re-written in terms of understeer gradient K_{us} and road curvature *R* can be re-written by using the kinematic relation between the yaw rate and the velocity of the vehicle as:

$$\delta = \frac{L\gamma}{v_x} + K_{us}a_y = \frac{L\gamma}{v_x} + \left(\frac{ml_r}{C_f L} - \frac{ml_f}{C_r L}\right)a_y, \quad (3.2)$$

where γ is the yaw rate, v_x is the longitudinal velocity, a_y is the lateral acceleration, m is the vehicle mass, and l_i is the distance between i^{th} tire and center of mass. The lateral tire force can be considered as linear relationship with the tire slip angle. However, the yaw rate can be seen as a momentary reaction of the system, which is not fitted to real vehicle, to steering wheel angle. In order to take into account the transient response of the cornering dynamics into the system, the lateral force of the tire is obtained from the vehicle's bicycle model as [Joa et al. 2018]

$$F_{yf} = \frac{ml_r}{L}a_y + \frac{I_z}{L}\dot{\gamma},$$
$$F_{yr} = \frac{ml_f}{L}a_y - \frac{I_z}{L}\dot{\gamma}, \quad (3.3)$$

where, I_z is the moment of inertia of vehicle. Substituted the lateral force in Equation 3.1 for Equation 3.3 and Equation 3.2 can be rewritten as:

$$\delta = \frac{L\gamma}{v_x} + \left\{\left(\frac{ml_r}{C_f L} - \frac{ml_f}{C_r L}\right) + \left(\frac{1}{C_f} - \frac{1}{C_r}\right) \cdot \frac{I_z \dot{\gamma}}{a_y L}\right\} a_y$$
$$= \frac{L\gamma}{v_x} + \{K_{us} + \Delta K_{us}\} a_y, \quad , \qquad (3.4)$$

where, ΔK_{us} is an added term, the transient term of understeer gradient, which is a function of yaw acceleration. Equation 3.4 can be expressed as including the transient response of system with the yaw acceleration. With small angle side-slip angle assumption and by re-organizing Equation 3.4, the desired yaw rate dynamics can be expressed as:

$$\dot{\gamma}_d = \frac{LC_f C_r}{I_z(C_f + C_r)} \cdot \left(\frac{L}{v_x} + K_{us} \cdot v_x\right) \gamma_d + \frac{LC_f C_r}{I_z(C_f + C_r)} \delta, \qquad (3.5)$$

where, γ_d is the desired yaw rate. γ_d can be resolved based on above dynamics which is the first-order dynamic relationship between steering angle and yaw rate. Therefore, how the desired yaw rate can result on the behavior of vehicle would be defined for the purpose to change the steer characteristics of vehicle. In other words, the amount of understeer or oversteer of vehicle can be changed by acquiring appropriate safety or agility of cornering performance.

3.1.3. Designing controller

To design a controller considering the characteristics of the entire vehicle system, the controller is divided into three steps. As shown in Figure 3.2, Supervisor with sensor and human request calculates target yaw rate in Equation 3.5 considered with vehicle bicycle model and linear tire model. This determines the yaw rate of vehicle to be tracked.

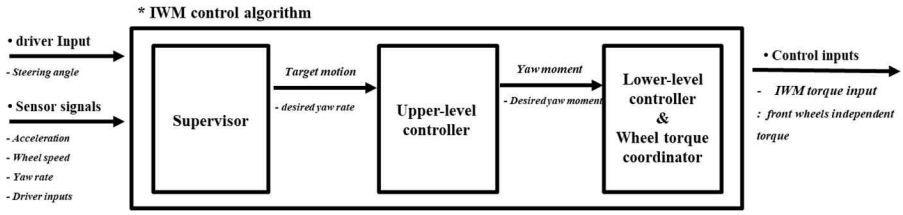

Figure 3.2 In-wheel Motor Control algorithm

In the case of the upper-level controller in Figure 3.2 , yaw rates determined by the supervisor are used to generate yaw moments for target motion in the upper-level controller. It is important how to design with feedback and feedforward terms in the controller using yaw dynamic for determined rates. The objective of the upper-level controller is to determine the desired yaw moment to reduce the yaw rate error between the actual yaw rate and the desired yaw rate. Due to model uncertainties and disturbances, the desired yaw moment is determined in the manner of a feedforward term only which is a similar scheme being previously chapter. The total yaw moment while the vehicle going to turning condition, can be a sum of the steady-state and transient yaw moment.

$$M_{z,total} = M_{z,ss} + M_{z,tr} \quad (3.6)$$

Where, $M_{z,ss}$ is the steady-state yaw moment, and $M_{z,tr}$ is the transient yaw moment while the vehicle goes into the turning event. In order to find the steady-state yaw moment $M_{z,ss}$ of the vehicle, the yaw moment with and without IWMs (base vehicle) can be defined and calculated. The required steering angle can be rewritten with the conventional kinematic relationship in bicycle model,

$$\delta_f = \left(\frac{L}{v_x} + K_{us,base}\, v_x\right)\gamma_{base} \quad (3.7)$$

Where, $K_{us,base}$ is the understeer gradient and γ_{base} is the yaw rate without IWMs. The kinematic model with IWMs including the steady-state yaw moment $M_{z,ss}$ can be expressed as

$$\delta_f = \left(\frac{L}{v_x} + K_{us,base}\, v_x\right)\gamma_{IWM} - \frac{M_{z,ss}}{A} \quad (3.8)$$

Using Equation 3.7 and 3.8, the steady-state yaw moment with IWM can be designed as

$$M_{z,ss} = A \cdot \left[K_{us,base} - K_{us,des}\right]a_y \quad (3.9)$$

where, $A = 2C_fC_rL/(C_f + C_r)$. The goal of the steady-state yaw moment is to modify the understeer gradient to fulfill the drivers' desires: Agile maneuver at the low speed (decrease the understeer gradient) and stable maneuver at the high speed (increase the understeer gradient).

Theorem 3.1. With the steady-state control input in Equation 3.9, the following statement holds. If the steady-state yaw moment $M_{z,ss}$ satisfies the control input constraints, then the steady-state yaw moment modifies the understeer gradient from $K_{us,base}$ to $K_{us,des}$.

(proof) Replacing $M_{z,ss}$ in the Equation 3.8 with the Equation 3.9, the kinematic model with the understeer gradient $K_{us,des}$ can be found.

In Equation 3.6 to determine the transient yaw moment $M_{z,tr}$, the bicycle model with the lateral acceleration can be considered. The bicycle model with the control inputs in state space, the side slip angle β and the yaw rate γ can be written as

$$\dot{\beta} = a_{11}\beta + a_{12}\gamma + b_1\delta_f$$
$$\dot{\gamma} = a_{21}\gamma + a_{22}\beta + b_2\delta_f + M_z/I_z \quad (3.10)$$

where, a_i and b_i are the coefficient of dynamic equation of the slip angle and yaw rate. Using the relationship between the lateral acceleration and kinematic bicycle model, Equation 3.10 with lateral acceleration can be expressed as,

$$a_y = v_x \cdot (\dot{\beta} + \gamma)$$
$$\frac{a_y}{v_x} = a_{11}\beta + (a_{12} + 1)\gamma + b_1\delta_f \quad (3.11)$$

Therefore, the transient yaw moment controller can be determined using the Laplace Transform of Equation 3.11,

$$\frac{\gamma}{\delta}(s) = \frac{1}{\tau s + 1}\left[\frac{v_x}{L}\left(1 + \frac{1}{A}\frac{M_z}{\delta_f}(s)\right) - \frac{K_{us}v_x}{L}\frac{a_y}{\delta_f}(s)\right] \quad (3.12)$$

where, τ is $(v_x I_z)/LA$ and A is $2C_fC_rL/(C_f + C_r)$. The steady-state response of Equation 3.12 is identical to that of the kinematic model of IWMs in Equation 3.8.

Remind that the proposed yaw moment is the sum of the steady-state yaw moment, which is in Equation 3.9, and the transient yaw moment. As described in Theorem 1, the steady-state yaw moment modifies the understeer gradient. The rest of the chapter will describe the design of the transient control input.

The transient yaw moment in this paper is aimed at modifying the transient response of the vehicle. The transient characteristics are parameterized with the time delay τ of the model in Equation (3.12). If the time delay τ increases,

the transient response becomes sluggish. In contrast, if the time delay τ decreases, the transient response becomes agile.

The goal of the transient control input is to change the time delay τ to $\eta\tau$. In summary, I devise the transient control input that transforms the original dynamics in Equation 3.12 to the dynamics with the time delay $\eta\tau$ as follows.

In Equation 3.12, the yaw moment M_z can be considered as the fraction of the steady-state yaw moment $M_{z,ss}$ because the transient yaw moment highly depends on time can be linearized with the lateral acceleration in kinematic model. Therefore, Equation 3.12 can be rewritten as

$$\frac{\gamma}{\delta}(s) = \frac{1}{\eta\tau s + 1}\left[\frac{v_x}{L}\left(1 + \frac{1}{A}\frac{M_{z,ss}}{\delta_f}(s)\right) - \frac{K_{us}v_x}{L}\frac{a_y}{\delta_f}(s)\right] \quad (3.13)$$

Adding Equation 3.12 to 3.13 and rearranging for the yaw moment, the final equation on s-domain can be

$$\begin{aligned}\frac{M_z}{\delta}(s) = A\left[\left(\frac{1}{\eta} - 1\right) + \frac{1}{\eta A}\frac{M_{z,ss}}{\delta_f}(s) + K_{us}\left(1 - \frac{1}{\eta}\right)\frac{a_y}{\delta_f}(s)\right. \\ \left. + \frac{L}{v_x}\left(1 - \frac{1}{\eta}\right)\frac{a_y}{\delta_f}(s)\right]\end{aligned} \quad (3.14)$$

In order to find a control law in time domain, Equation 3.14, the proposed control input, can be reformed by inverse Laplace Transform and rewritten as

$$\begin{aligned}M_z = A\left[\left(1 - \frac{1}{\eta}\right)\delta_f + \left[K_{us,des}\left(1 - \frac{1}{\eta}\right) + \frac{1}{\eta}\Delta\mathrm{K_{us}}\right]a_y\right. \\ \left. + \frac{L}{v_x}\left(1 - \frac{1}{\eta}\right)\gamma\right]\end{aligned} \quad (3.15)$$

Where, $\Delta\mathrm{K_{us}}$ is the difference between $K_{us,base}$ and $K_{us,des}$ and η is a design parameter for tuning which can change the transient yaw rate response

depends on the steering angle input.

Theorem 3.2. With the proposed control input in Equation 3.15, the following statement holds. If the proposed yaw moment M_z satisfies the control input constraints, then the proposed yaw moment modifies not only the understeer gradient from $K_{us,base}$ to $K_{us,des}$ but also the time delay from τ to $\eta\tau$.

(proof) Replacing M_z in the Equation 3.12 with the Equation 3.14, we can get the dynamic model in Equation 3.13.

Therefore, the desired motion controller (upper-level controller) as shown in Figure 3.2, based on the error between the understeer gradient of original vehicle and calculated that of supervisor controller. The lower-level controller as shown in Figure 3.2 needs to control the in-wheel motor with the torque allocation from the input, the desired yaw moment.

The lower-level controller and wheel torque coordinator in Figure 3.2, receives the target yaw moment from the IWMs which is calculated by Equation 3.15.

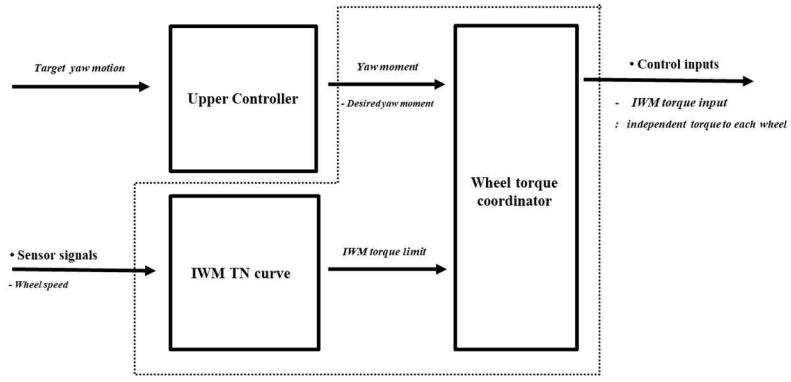

Figure 3.3 Lower-level controller and wheel torque coordinator

Using the map of T-N (torque-rotational speed) curve for IWMs, and the desired yaw moment, the wheel torque can be allocated to the left and right wheels. In this chapter, front IWMs system is considered to validate the dynamic torque vectoring controller. Therefore, the torque of front right side of wheel can be calculated as

$$\Delta \mathrm{T} = M_{z,des}\frac{r_{eff}}{t_{wt}}$$
$$T_{total,fl} = T_{bngi} - \Delta T \quad (3.16)$$
$$T_{total,fr} = T_{bngi} + \Delta T$$

where, T_{fr} is the torque applied to front right wheel, T_{fl} is the torque applied to front left wheel, r_{eff} is the effective radius of tire, and t_{wt} is the track width of vehicle.

3.2. Validation with Simulation and Experiment

3.2.1. Simulation

Simulation studies can be done to verify the outstanding results of the proposed controller which has the understeer gradients of the vehicle, with CARSIM, the vehicle dynamics software, and MATLAB/Simulink. The vehicle model is a Hyundai Genesis sedan. The powertrain consists of front two IWMs and internal combustion engine with rear wheel driven system. The tire model can be used as the Magic Formular tire model [Pacejka 2005]. The vehicle parameters are given in table 3.3.

Symbol	Parameter	Value
m	Total vehicle mass	1960 kg
l_f	CG-front axle distance	1.319 m
l_r	CG-rear axle distance	1.517 m
TGR	Total steer gear ratio	12.8
H_{cg}	Height of CG	0.57 m
$t_{w\,t}$	Track width	1.630m (F), 1.650m(R)
C_f	Tire cornering stiffness of front axle	120,000 N/rad
C_r	Tire cornering stiffness of rear axle	120,000 N/rad
L	Wheelbase	2.836 m
$P_{m\,ax}$	Maximum power of IWMs	30 KW
$T_{m\,ax}$	Maximum Torque of IWMs	650 Nm
$m_{unsprung}$	Additional unsprung mass	42.4 kg
I_z	Yaw moment of inertia	2800 kgm^2
r_{eff}	Effective tire radius	0.33 m

Table 3.3 Vehicle specification for simulation study

To find effects of the steady-state condition, a circular turn test can be conducted with gradual acceleration until saturation of tire and constant radius turn test. The transient response of the DTV controller can be shown using step steer test with open loop test. In those simulation test, yaw motion and understeer characteristics can be observed with vehicle speed and lateral acceleration. As shown in Figure 3.4, the base model (blue dot line) without

DTV controller, has the characteristics of a typical understeer vehicle, which shows a gradual increase in steering angle as the vehicle speed increases. However, unlike the base model, DTV controller (red solid line) has a relatively low rate of increase in steering angle, which reduces understeer, despite changes in vehicle speed, rate, and lateral acceleration being similar to the basic model. Another notable point is that at vehicle speeds above 70 km/h, the steering angle of models with DTV controllers increases, which is due to the limitations of the DTV actuators, resulting in an additional reduction in torque generation.

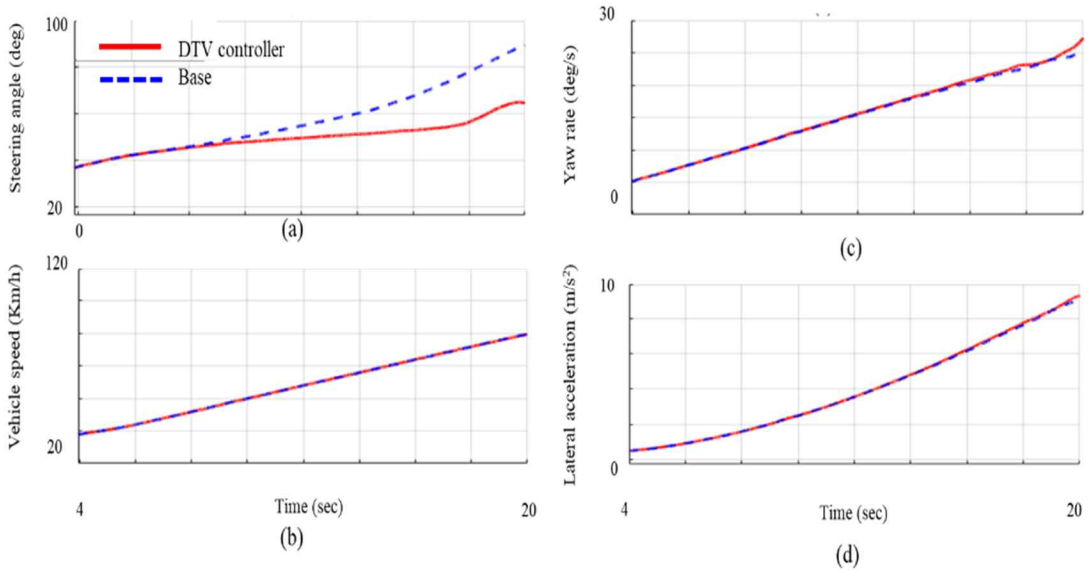

Figure 3.4 Circular turn simulation with R 50 m on dry asphalt (μ= 0.9)

Figure 3.5 shows that the simulation result of constant radius turn test with relationship between the lateral acceleration and steering wheel angle to find understeer gradients of the DTV controller.

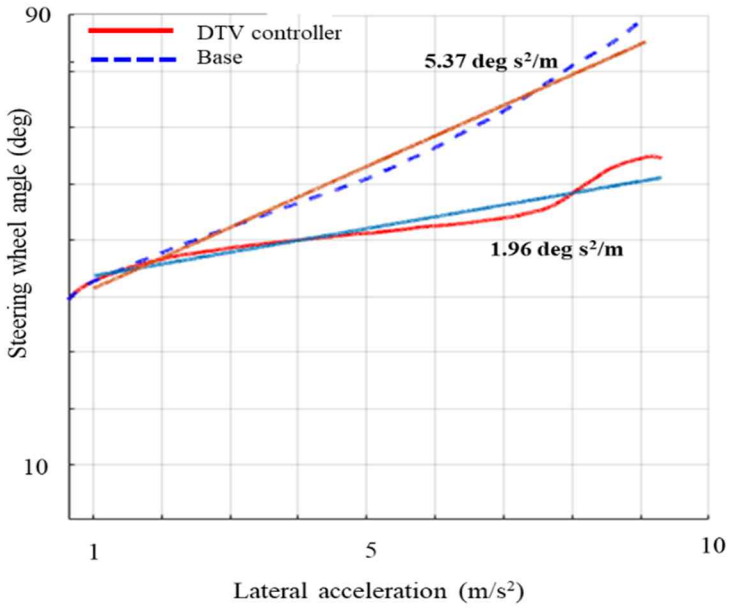

Figure 3.5 Comparison of understeer gradient with DTV controller

The effect of DTV control on operation shows that through linear curve fittings, 63.5% of the decrease in the understeer gradient with lateral acceleration compared to base vehicles has been improved. With lateral acceleration above 7.7 m/s^2, the DTV controller can be seen to have reached the limit of the motor of the IWMs due to the influence of the high front wheel speed, resulting in additional understeer. As a result of Figure 3.5, it is shown that the DTV controller directly controls the understeer slope, causing significant changes in the understeer characteristics that affect the steady-state handling performance of the vehicle.

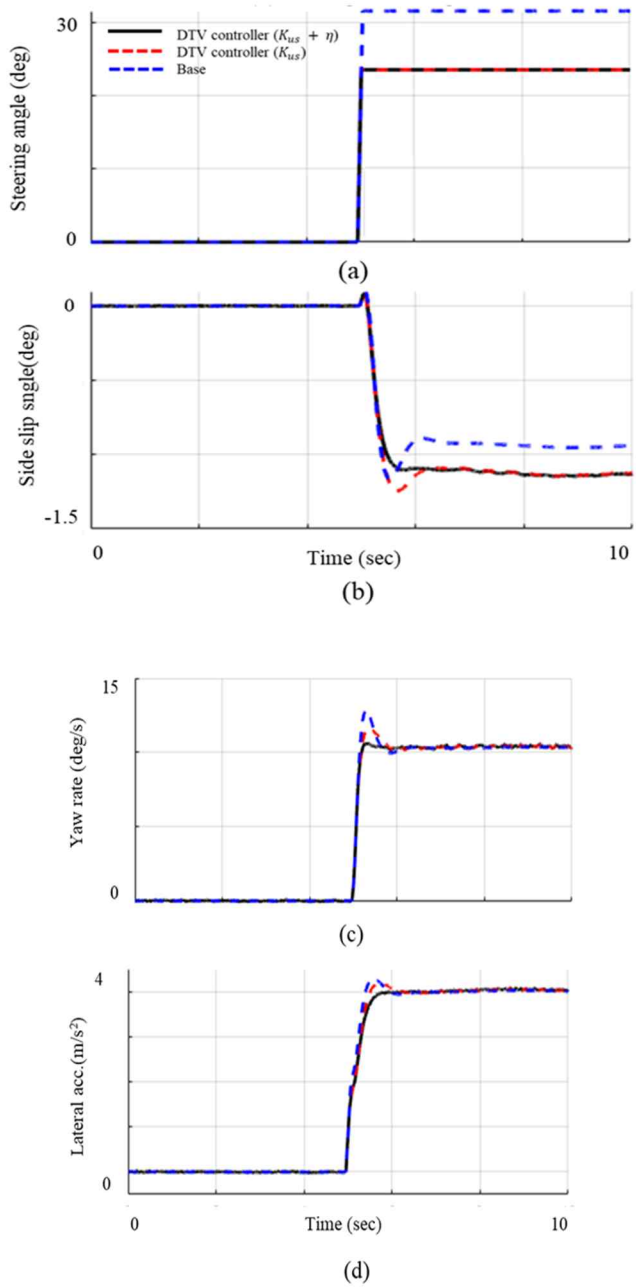

Figure 3.6 Simulation 80kph, Step steer test, Lateral acc. = 0.4g

Figure 3.6 shows that the simulation results from step steer test for full vehicle model with DTV controller which has the term K_{us}, steady-state understeer gradient controller and the term η , transient controller with first order delay model with time constant. Figure 3.6 (a) illustrates that compared the base model, DTV controller significantly reduced the steering angle when the same lateral acceleration and steady-state yaw rate due to the understeer gradient term K_{us}. Figure 3.6 (b), (c) and (d) shows that the DTV controller can be seen in step steer tests as a characteristic of damping, which affects the overshoot of the yaw rate and the side slide angle. Comparing the Full DTV Controller (black solid line) and the steady-state DTV Controller (red dotted line) shows that the overshoot of the yaw rate, side slip angle is significantly reduced. This simulation results can be seen as the effect of the first order delay model and tuning factor η, introduced to consider the transient characteristics induced Equation 3.15 in the previous section, indicating that the DTV controller has a very good performance in both steady-state and transient state, resulting in a simulation of dynamic torque vectoring characteristics with the vehicle.

3.2.2. Vehicle Experiment

In this section, the performance of the previously designed DTV controller is to be experiment and tested using a real vehicle. The vehicle is Hyundai's luxury sedan, a four-wheel drive vehicle with rear-wheel drive and front-wheel in-wheel system. The maximum torque and power of the engine are 343.23 Nm and 211.5 kW, respectively. Excluding the total gear ratio N, those of IWMs are 74.7 Nm and 30 kW, respectively. Total maximum wheel torque of IWMs can be calculated as 650 Nm using reduction gear ratio 8.74. In Figure 3.7 shows the experimental set-up, such as experimental vehicle, DGPS, IWMs, Micro-

Autobox, battery system and data acquisition system. The DGPS from Oxford Technical Solution is a high-precision differential GPS system, so that the sideslip angle and yaw rate measured by RT3002 is regarded as an actual value. This device is located close CG of the vehicle. The specifications of the experimental vehicle are presented in table 3.3.

The sampling time of each sensor is 1 ms for DGPS and 10ms for in-vehicle sensor. On the controller area network (CAN), the overall algorithm built into the mAutobox runs with a sampling time of 10 ms.

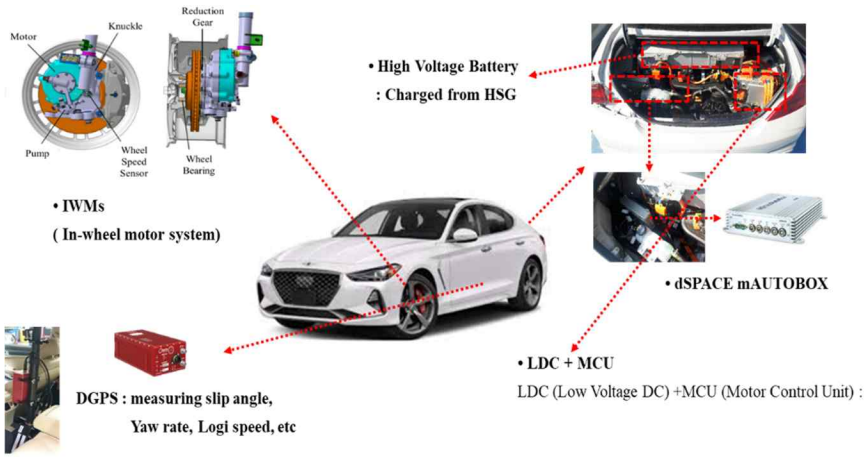

Figure 3.7 Experimental environment

The experimental test conducted the constant radius test, one of the open loop tests specified in ISO 4138, to see the effectiveness of the basic designed steady-state state of DTV control and the double lane change test, which is a test item in ISO 3888-1 for transient response.

A. Open-loop constant radius test

The constant radius test method can be divided into two ways. In the first, it can be carried out by keeping the constant speed of the vehicle and

discretely increasing the speed to acquire motion data of the vehicle and continuously increasing the speed of the vehicle on the circular path. Here, the latter method was carried out. The first scenario was one of tests in ISO 4138, an open-loop circular turn test with constant acceleration without changing the radius of circle. The radius of circle is 50 meters, and the acceleration has been exerted until the tire saturated. This scenario can be time-effective than steady-state circular test with discrete speed, even the results can be considered as the steady-state turning event to be analyzed. Figure 3.9 shows that the open-loop constant radius vehicle test with and without DTV. Figure 3.9 (a) variation of steering wheel angle and (b) the longitudinal velocity with time illustrates the significant reduction of understeer gradient with DTV controller.

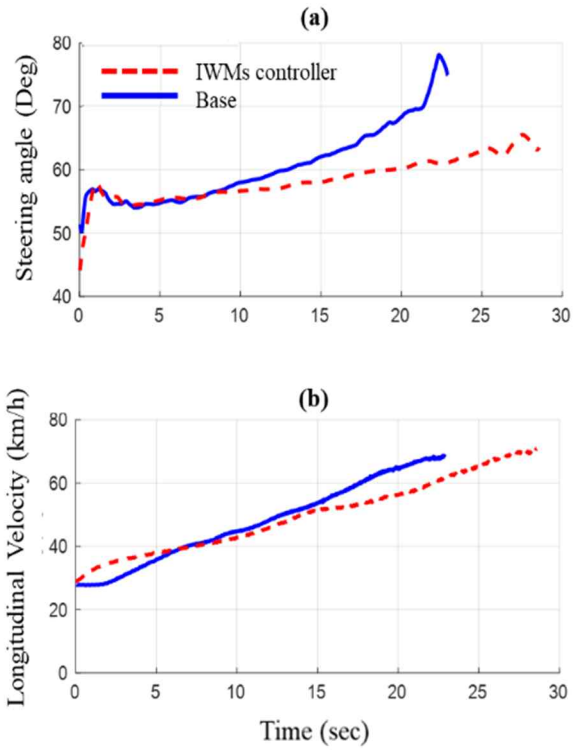

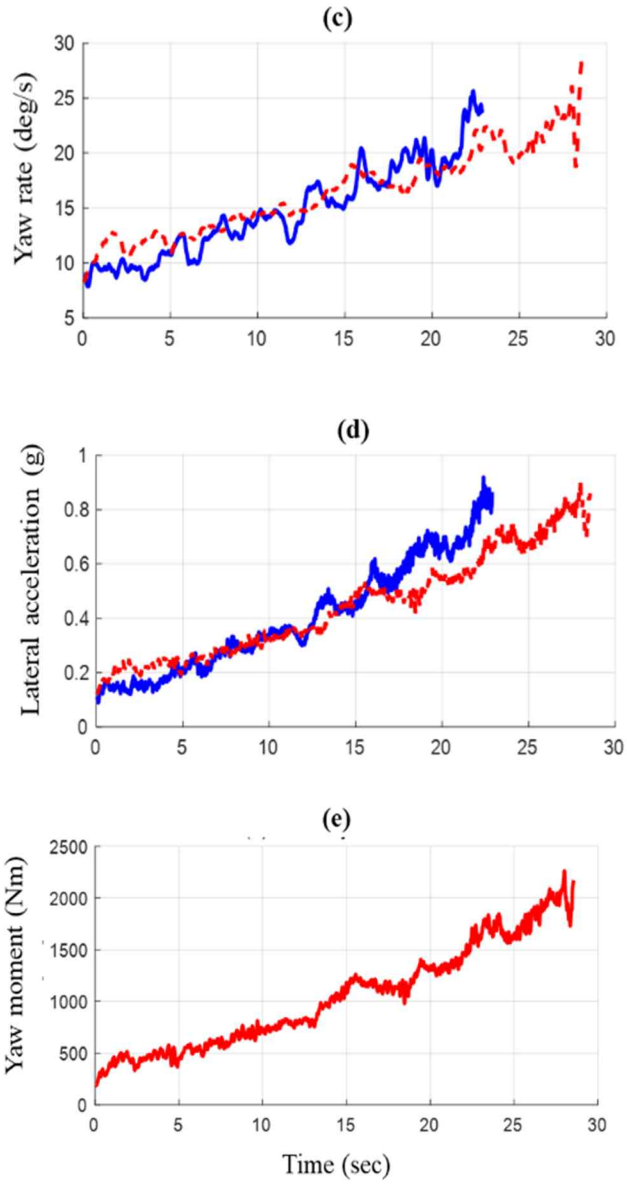
(c)
Yaw rate (deg/s)
30
25
20
15
10
5
0
5
10
15
20
25
30
(d)
Lateral acceleration (g)
1
0.8
0.6
0.4
0.2
0
0
5
10
15
20
25
30
(e)
Yaw moment (Nm)
2500
2000
1500
1000
500
0
0
5
10
15
20
25
30
Time (sec)

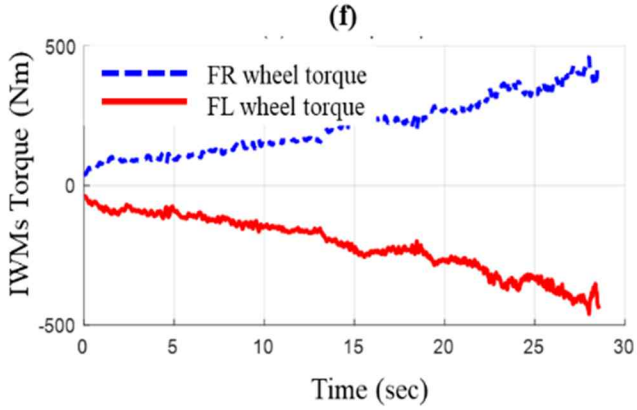

Figure 3.8 Constant radius test with and without DTV

Figure 3.9 (e) and (f) shows that desired yaw moment calculated on DTV controller between target and measured understeer gradient increases using added the front right and left IWMs torque.

The understeer gradient with activated DTV controller as shown in Figure 3.9 is significantly reduced with a tendency very similar to the simulation results in the previous section. Using the linear curve fitting, without DTV, K_{us} is 0.046 rad/g, K_{us} on activated DTV is 0.0214 rad/g. The reduction of understeer gradient is 54% as similar as the simulation result.

B. Closed-loop double lane change test.

Another experiment scenario is one of severe lane change maneuver vehicle

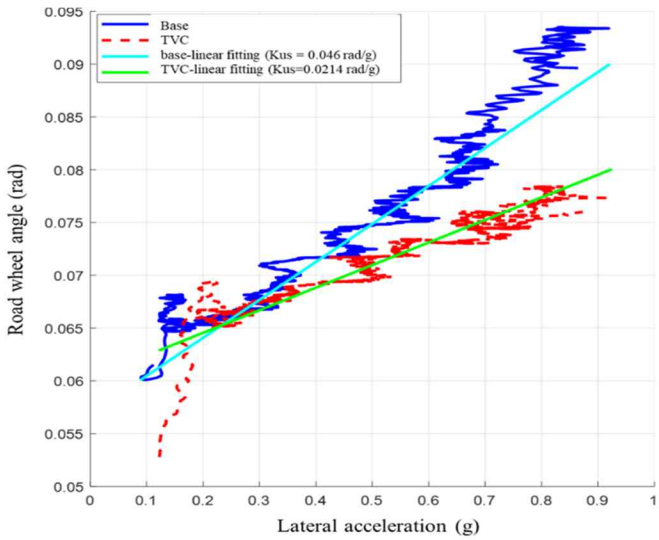

Figure 3.9 Comparison of understeer gradient with base and DTVC.

tests to analyze closed-loop transient response of the DTV controller. The test procedure of double lane change test based on ISO 3888-1, can be conducted. This kind of test can be a closed-loop test which evaluate the dynamic behavior of a road vehicle, the significant interaction of these driver-vehicle-environment elements. The main purpose of the severe double lane-change maneuver is a dynamic process consisting of rapidly driving a vehicle from its initial lane to another lane parallel to the initial lane, and returning to the initial lane, without exceeding lane boundaries. Figure 3.10 shows that the dimension of the track and designation of section with vehicle test procedure. based on ISO 3888-1. Although the test was developed for testing lateral dynamics, it was found that the longitudinal dynamics had a strong influence, which explained a considerable amount of scatter in the data and thus reflected on the

results. Therefore, this test is a very suitable scenario for evaluating the newly designed DTV controller on impregnated IWMs vehicles.

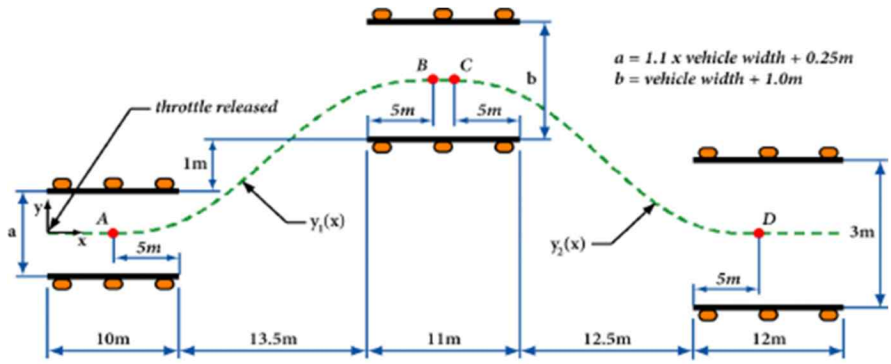

Figure 3.10 Double lane change test based on ISO 3888-1

Figure 3.11 shows that the test results with double lane change maneuver compare between the vehicle with and without DTV controller. The steering angle is reduced by the effects of the controller with K_{us} and the longitudinal velocity is higher than base vehicle as shown in Figure 3.11 (a) and (b). The yaw damping effect from DTV controller shows the yaw rate of peak to peak is reduced than base test in Figure 3.11 (c). Finally, one of important parameters in the test, the sideslip angle significantly is reduced from eighteen degrees to ten degrees in peak-to-peak values as shown in Figure 3.11 (e). It means that reduced sideslip angle helps increasing the longitudinal velocity about 5 Km/h and improving stability of vehicle handling.

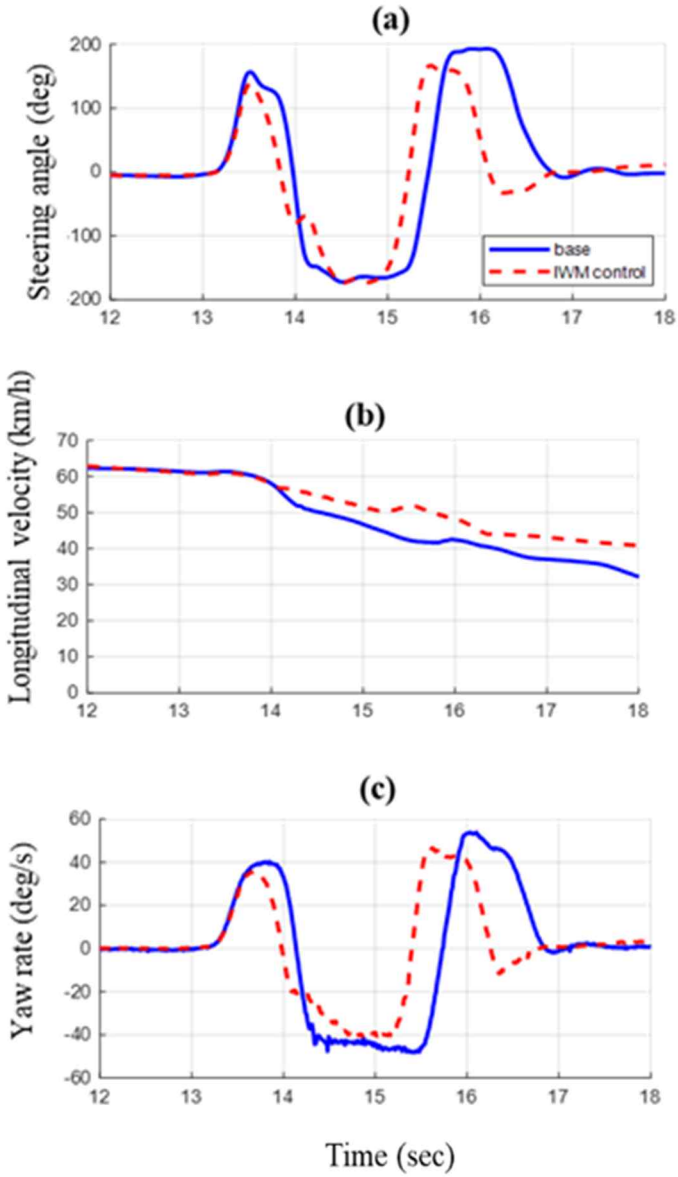
(a)
Steering angle (deg)
200
100
0
-100
-200
12
13
14
15
16
17
18
base
IWM control
(b)
Longitudinal velocity (km/h)
70
60
50
40
30
20
10
0
(c)
Yaw rate (deg/s)
60
40
20
0
-20
-40
-60
Time (sec)

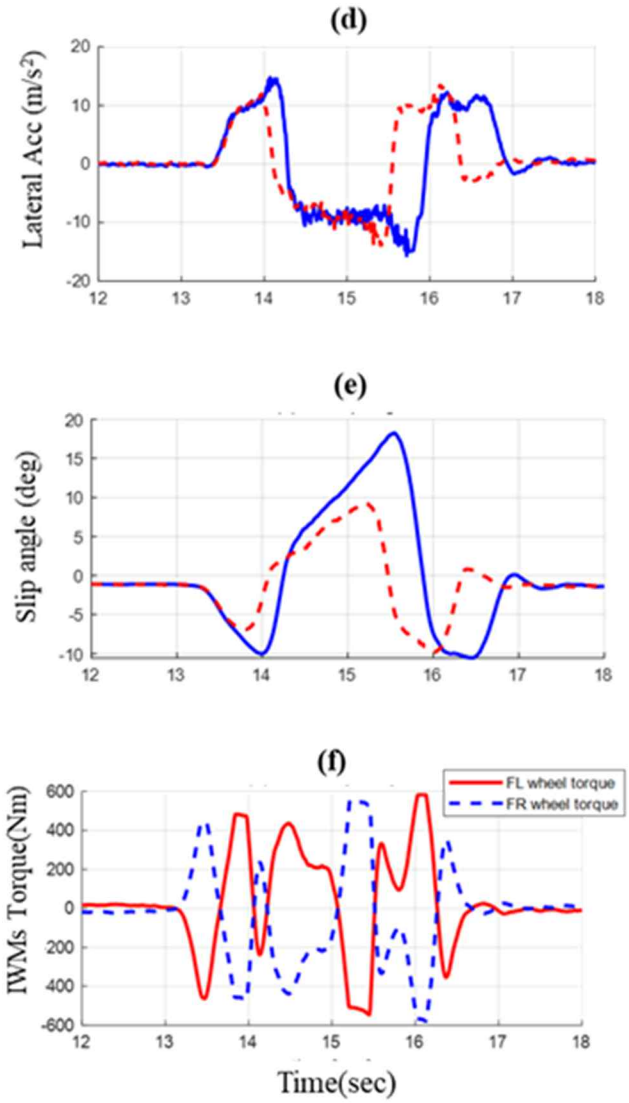

Figure 3.11 Test results of double lane change maneuver of vehicle

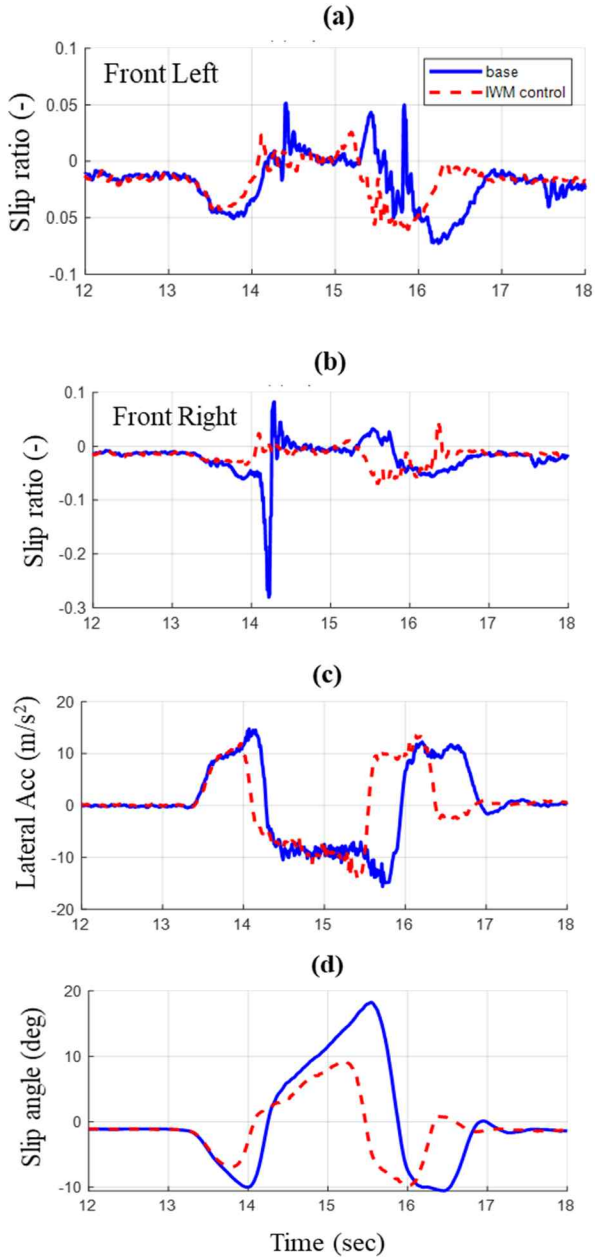

Figure 3.12 Comparison of the slip ratio for front left and right wheels

Figure 3.12 shows that the comparison between base with and without TV controller can be plotted for the slip ratio of front left and right wheels. After the first lane changing maneuver, the right wheel of base vehicle can be seen as the saturation of tire at 14.2 seconds of test in Figure 3.13 (b). The reason that the right wheel can be changed from outside to inside wheel on cornering condition, then the slip ratio of the right wheel increases significantly. It means that TV controller works on reduced steering angle and small sideslip angle of the vehicle thus the slip ratio of tires can be kept small numbers, which can be considered as securing the margin of tire saturation.

Using the full vehicle test with several scenarios, proposed algorithm for TV control has been validated and performed successfully in steady-state and transient driving condition. The four motor IWMs system can be delt with the following chapter with multiple sliding control technique and optimization methods.

Chapter 4 Dynamic handling control for Four-wheel Drive In-Wheel platform

IWMs vehicles have many advantages, such as energy efficiency and changes in vehicle motion. The response is speedy and accurate, mainly because it directly applies torque to the driveline. Moreover, the independent control of each of the four wheels of the system, in the vehicle's motion and dynamic posture, can be controlled with the desired handling characteristics. Based on these benefits, over the past few years, enormous research on the advanced dynamics control of electric vehicles has been performed [Sakai, Sado, and Hori 1999, Yin, Oh, and Hori 2009, Mutoh and Nakano 2011, Chen and Wang 2011, Wang and Wang 2011]. The purpose of the state-of-the-art motion control study is to preserve stability and controllability by reducing unexpected vehicle behavior with active vehicle control. The main control objective of the motion control system is to control input such as zero-yaw rate, zero-sideslip, and prevention of roll-over by implementing a chassis control system including differential braking, active steering, and suspension. Chapter 2 uses a discrete sliding controller to maintain a constant vehicle rate and sideslip angle in extreme case drift handling in-vehicle limit turn handling, which can be used to increase vehicle agility and controllability in Fun-to-drive mode for high-performance electric vehicles. The result of the controller with the steady-state understeer gradient and transient control parameters shown in Chapter 3 is that

IWMs are applied to the front two wheels of the vehicle so that when the vehicle is in an unstable state, the vehicle can now be implemented in a Safe-driving mode. Therefore, in this chapter, dynamic torque vectoring control with a four-wheel motor system with Multiple Adaptive Sliding Mode Control (MASMC) approach is composed of a yaw rate controller and sideslip angle controller. Consequently, there are two types of driving modes, the safety mode and the dynamic mode. MASMC can be used in torque vectoring technology to improve the handling performance of fully electric vehicles.

4.1. Vehicle System Modeling

In this section, the introduction of a 3-DOF yaw plane model describes the lateral behavior of an electric vehicle with a four-wheel motor that can be driven independently and has an active front steering system. Figure 2.1 illustrates a simplified yaw plane model is used for the control design of dynamic torque vectoring control.

The governing equations for lateral motions are given by Equations 2.27-2.29. Using a linear tire model, the dynamic equation for side-slip angle and yaw rate can be expressed as follows:

$$\dot{\beta} = -\frac{2\left(C_f + C_r\right)}{mv_x}\beta + \left(\frac{2\left(l_r C_r - l_f C_f\right)}{mv_x^2} - 1\right)\gamma + \frac{2C_f}{mv_x}\delta_f \qquad (4.1)$$

$$I_z\dot{\gamma} = -\frac{2\left(l_f^2 C_f + l_r^2 C_r\right)}{v_x}\gamma + 2\left(l_r C_r - l_f C_f\right)\beta + 2l_f C_f \delta_f + M_z \qquad (4.2)$$

This study can control yaw rate by the yaw moment M_z in the yaw rate dynamic. Then, we can also control the side-slip angle by yaw rate in the side-

slip angle dynamic. To summarize, we have designed the cascade structure for side-slip angle control; thereby, we can create the divided controllers according to the safety driving mode and dynamic driving mode. The safety mode is a basic mode of a motion control system that forces the vehicle to maintain a stable yaw rate by intercepting the side-slip angle controller. In contrast, dynamic mode, which is based on side-slip angle control, is a selective option where both system and driver make decisions for which they require dynamic mode for improved handling.

Equation 4.1 and 4.2 can be rearranged in state space form as follows:

$$\dot{x}(t) = Ax(t) + Bu$$
$$y(t) = Cx(t) \tag{4.3}$$

where $x = [\beta, \gamma]^T, u = \left[\delta_f, M_z\right]^T, y = \beta$, and

$$A = \begin{bmatrix} \dfrac{-2\left(C_f + C_r\right)}{mv_x} & \dfrac{2\left(l_r C_r - l_f C_f\right)}{mv_x^2} - 1 \\ \dfrac{2\left(l_r C_r - l_f C_f\right)}{I_z} & \dfrac{-2\left(l_f^2 C_f - l_r^2 C_r\right)}{I_z v_x} \end{bmatrix}$$
$$B = \begin{bmatrix} \dfrac{2C_f}{mv_x} & 0 \\ \dfrac{2l_f C_f}{I_z} & \dfrac{1}{I_z} \end{bmatrix}, \qquad C = [1 \quad 0] \tag{4.4}$$

In this state-space form, two states sideslip angle, β and yaw rate, γ, control inputs, steering angle δ_f and yaw moment M_z can be considered. In the real world, vehicle speed, v_x can be changed widely and cornering stiffness $C_{f,r}$ have also some variations in environmental conditions, such as change of

weight, level of road friction, temperature, and so on. The parameters do not include all non-linear characteristics of tire as well. Therefore, a robust controller can be introduced to prevent undesirable effects.

Figure 4.1 shows the proposed control scheme for multiple adaptive sliding mode control (MASMC), a selective option for driver intention, safety, and fun-to-drive priority. The system includes model-based generators which create the desired vehicle lateral acceleration, yaw rate and sideslip angle, and an outer adaptive sliding mode control (ASMC) for the reference yaw rate, and inner adaptive sliding mode control algorithm for generating the yaw moment, a torque distribution law for minimizing actuator redundancy. Finally, a CarSim vehicle model with simulation for verification of the performance of the proposed MASMC.

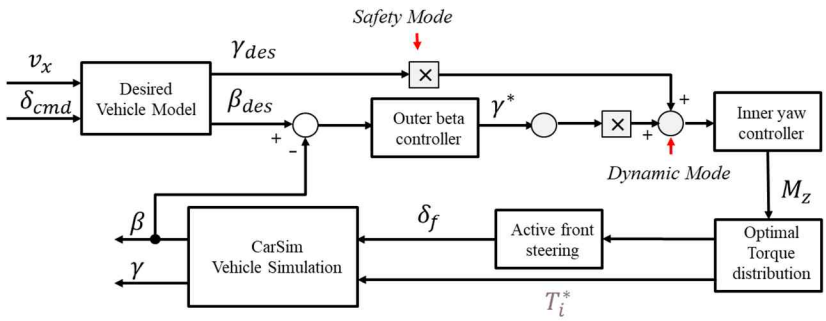

Figure 4.1 Overall control scheme of proposed MASME

4.2. Motion Control based on MASMC

In this section, vehicle motion control's main purpose is deeply related to improving vehicle cornering performance and keeping stability under various driving behavior and environments. For cornering maneuvers, side-slip angle

β of the vehicle should be close to the desired vehicle responses, and the desired yaw rate γ is required for safety. The desired vehicle responses are based on the driver's cornering intention (i.e., driver's steering command and vehicle velocity). Commonly, $\dot{\beta} = \dot{\gamma} = 0$ during steady-state cornering. The desired vehicle lateral acceleration, yaw rate and side- slip angle are defined as follows:

$$a_{y,des} = v_x(\gamma_d + \dot{\beta}_d) \tag{4.5}$$

$$\gamma_d = \frac{1}{1+\tau_\gamma} \cdot \frac{1}{1+K_s v_x^2} \cdot \frac{v_x}{l} \cdot \delta_{cm\,d} \tag{4.6}$$

$$\beta_d = \frac{1}{1+\tau_\beta} \cdot \frac{1-\left(\frac{m l_f v_x^2}{2 l l_r C_r}\right)}{1+K_s v_x^2} \cdot \frac{v_x}{l} \cdot \delta_{cm\,d} \tag{4.7}$$

$$K_s = \frac{m(l_r C_r - l_f C_f)}{2 l^2 C_f C_r} \tag{4.8}$$

where τ_γ and τ_β are the relaxation time constants of the desired model filters, and K_s is the vehicle stability factor, which describes the steering characteristics of the vehicle, which are classified as follows:

$$\begin{cases} l_r C_r - l_f C_f > 0, & understeer \\ l_r C_r - l_f C_f = 0, & neutral\ \ steer \\ l_r C_r - l_f C_f < 0, & oversteer \end{cases} \tag{4.9}$$

4.2.1. Yaw motion controller for the inner ASMC

In general, tracking the sideslip angle associated with the vehicle's posture in an area where the car performs lane change or cornering is a very tricky control. The dynamic performance of the vehicle's motion changes is due to the vehicle's control parameters, such as vehicle speed, yaw rate, and lateral acceleration, being influenced by the high nonlinear characteristics of parts such as the vehicle's tires, steering, and suspension characteristics. To perform these high nonlinear system controls, such as the drift control, discussed in Chapter 2, similarly sliding mode control techniques are effective control techniques that can overcome external disturbances and inaccuracies in the vehicle's model, enabling stable control with fast response characteristics [Shen et al. 2018] [Mutoh, Kazama, and Takita 2006].

With similar way in Chapter 2, the control makes the system to slide on a certain surface which guarantees the achievement of the control objective. To achieve the inner control objective which is tracking the reference yaw rate made by outer SMC (i.e., $\lim_{t\to\infty} s_\gamma(t) = 0$), the sliding surface $s_\gamma(t)$ is defined as

$$s_\gamma \triangleq \gamma - \gamma_d \tag{4.10}$$

The sliding surface $s_\gamma(t) = 0$ denotes no tracking error of yaw rate. The time derivative of Equation 4.10, yields

$$\dot{s}_\gamma = \dot{\gamma} - \dot{\gamma}_d \tag{4.11}$$

Using Equation 4.2 and 4.11 yields,

$$\dot{s}_\gamma = -\frac{2\left(l_f^2 C_f + l_r^2 C_r\right)}{I_z v_x}\gamma + \frac{2\left(l_r C_r - l_f C_f\right)}{I_z}\beta + \frac{2 l_f C_f}{I_z}\delta_f + \frac{M_z}{I_z} + \frac{M_d}{I_z} - \dot{\gamma} d \quad (4.12)$$

where M_d is newly defined as a yaw moment of the disturbance mainly caused by lateral wind and unbalanced road conditions. To achieve the control requirement, a reaching surface to be satisfied is designed as follows:

$$\dot{s}_\gamma = -k_{p\gamma} s_\gamma - k_{s\gamma} \cdot sgn\left(s_\gamma\right) \quad (4.13)$$

where $k_{p\gamma}$ and $k_{s\gamma}$ are the positive control parameters selected to decide reaching speed and convergence rate of a tracking error. Additionally, $k_{s\gamma}$ should be tuned according to boundaries of uncertainties and disturbances. The inner sliding mode control law M_z derived from Equations 4.12 and 4.13 is

$$M_z = I_z \dot{\gamma}_d + \frac{2B}{v_x}\gamma + 2A\beta - 2 l_f C_f \delta_f - I_z k_{p\gamma} s_\gamma - I_z k_{s\gamma} \cdot sgn\left(s_\gamma\right) \quad (4.14)$$

where A is defined as a yaw spring coefficient (i.e.,$A = l_r C_r - l_f C_f$) and B is defined as a yaw damping coefficient (i.e., $B = l_f^2 C_f + l_r^2 C_r$), which vary with cornering stiffness.

There are two types of model uncertainties, unmodeled nonlinear dynamic uncertainties such as assumptions for calculation simplification and parametric uncertainties such as varying parameters. In designing an SMC, only a robust term like signum or saturation function overcomes these two model uncertainties to obtain robust stability. The model uncertainties, especially the parametric uncertainties, increase the gain of these robust terms to obtain the same tracking performance. As a result, the higher gain creates unnecessary

chattering, causing uncomfortable feelings to drivers. To reduce the high gain chattering due to varying parameters, we applied adaptive control strategy. Thus, the control law M_z is modified as

$$M_z = I_z\dot{\gamma}_d + \frac{2\hat{B}}{v_x}\gamma + 2\hat{A}\beta - 2l_f\hat{C}_f\delta_f - k_{p\gamma}s_\gamma - k_{s\gamma}\cdot sgn\left(s_\gamma\right) \quad (4.15)$$

where, the adaptation laws for the updated parameters $\hat{A}, \hat{B}$ and $\hat{C}_f$ are chosen as

$$\hat{A}(t) = -\frac{2k_1}{I_z}\beta(t)s_\gamma - \eta_1 k_1\tilde{A}$$

$$\hat{B}(t) = -\frac{2k_2}{I_z v_x}\gamma(t)s_\gamma - \eta_2 k_2\tilde{B} \quad (4.16)$$

$$\hat{C}_f(t) = -\frac{2k_3 l_f}{I_z}\delta_f(t)s_\gamma - \eta_3 k_3\tilde{C}_f$$

where, $\tilde{A} = \hat{A}(t) - A, \tilde{B} = \hat{B}(t) - B, \tilde{C}_f = \tilde{C}_f(t) - C, k_i(i = 1,2,3)$ is the positive constant adaptation gain which determines the update rate and $\eta_i(i = 1,2,3)$ is the positive constant.

To prove the stability of the inner designed control system, the following positive definite Lyapunov function is considered.

$$V_1 = \frac{1}{2}s_\gamma^2 + \frac{1}{2k_1}\tilde{A}^2 + \frac{1}{2k_2}\tilde{B}^2 + \frac{1}{2k_3}\tilde{C}_f^2 \quad (4.17)$$

Taking the time derivative of Equation 4.17, substituting for $\dot{s_\gamma}$ from Equation 4.12, and plugging in the control law M_z and adaptation laws,

$$\dot{V}_1 = s_\gamma\,\dot{s_\gamma} + \frac{1}{k_1}\tilde{A}\dot{\hat{A}} + \frac{1}{k_2}\tilde{B}\dot{\hat{B}} + \frac{1}{k_3}\tilde{C}_f\dot{\hat{C}}_f \quad (4.18)$$

$$= s_\gamma \left[-\frac{2B}{I_z v_x}\gamma + \frac{2A}{I_z}\beta + \frac{2l_f C_f}{I_z}\delta_f + \frac{M_z}{I_z} + \frac{M_d}{I_z} - \dot{\gamma}d \right] + \frac{1}{k_1}\tilde{A}\dot{\hat{A}} + \frac{1}{k_2}\tilde{B}\dot{\hat{B}} + \frac{1}{k_3}\tilde{C}_f\dot{\hat{C}}_f$$

$$= s_\gamma \left[\frac{2\gamma}{I_z v_x}\tilde{B} - \frac{2\beta}{I_z}\tilde{A} - \frac{2l_f\delta_f}{I_z}\tilde{C}_f - k_{p\gamma}s_\gamma - k_{s\gamma}\cdot sgn\left(s_\gamma\right) + \frac{M_d}{I_z} \right] + \frac{1}{k_1}\tilde{A}\left(-\frac{2k_1}{I_z}\beta(t)s_\gamma - \eta_1 k_1 \tilde{A} \right) + \frac{1}{k_2}\tilde{B}\left(-\frac{2k_2}{I_z v_x}\gamma(t)s_\gamma - \eta_2 k_2 \tilde{B} \right) + \frac{1}{k_3}\tilde{C}_f\left(-\frac{2k_3 l_f}{I_z}\delta_f(t)s_\gamma - \eta_3 k_3 \tilde{C}_f \right)$$

$$\leq -k_{p\gamma}{s_\gamma}^2 - k_{s\gamma}|s_\gamma| + |s_\gamma|\cdot\left|\frac{M_d}{I_z}\right| - \eta_1\tilde{A}^2 - \eta_2\tilde{B}^2 - \eta_3\tilde{C}_f^2$$

Define $\Gamma = sup_{\,t\geq 0}\left|\frac{M_d}{I_z}\right|$. If $k_{s\gamma} > \Gamma$, Equation 4.18 can be rewritten as

$$\begin{aligned}\dot{V}_1 &\leq -k_{p\gamma}s_\gamma^2 - k_{s\gamma}|s_\gamma| + |s_\gamma|\cdot\left|\frac{M_d}{I_z}\right| - \eta_1\tilde{A}^2 - \eta_2\tilde{B}^2 - \eta_3\tilde{C}_f^2 \\ &= -k_{p\gamma}s_\gamma^2 - |s_\gamma|\cdot\left(k_{s\gamma} - \left|\frac{M_d}{I_z}\right|\right) - \eta_1\tilde{A}^2 - \eta_2\tilde{B}^2 - \eta_3\tilde{C}_f^2 \\ &\leq -k_{p\gamma}s_\gamma^2 - |s_\gamma|\cdot\left(k_{s\gamma} - \Gamma\right) - \eta_1\tilde{A}^2 - \eta_2\tilde{B}^2 - \eta_3\tilde{C}_f^2 < 0\end{aligned} \qquad (4.19)$$

The function $V_1(t)$ is a positive definite and $\dot{V}_1(t)$ is a negative semi-definite. Moreover, $V_1(t)$ tends to infinity as $S_\gamma(t)$ tends to infinity, therefore, because of Lyapunov's direct method, the equilibrium at the origin $S_\gamma(t) = 0$ is globally stable and the variable $S_\gamma(t)$ is bounded. To compound the above conclusions, we can prove that the stability of the proposed control

law, which is the satisfied control objective, i.e., $S_\gamma(t) \to 0$ as $t \to \infty$, according to Lyapunov stability theory.

4.2.2. Sideslip angle controller for the outer ASMC

As yaw motion controller in the inner ASMC design, the control makes the system slide on a certain surface which guarantees the achievement of the control objective. To achieve the outer control objective which is tracking the desired side-slip angle β, i.e., $\lim_{t\to\infty} s_\beta(t) = 0$, the sliding surface $s_\beta(t)$ is defined as:

$$s_\beta(t) \triangleq \beta - \beta_d \quad (4.20)$$

Then, we can see that the sliding surface $s_\beta(t) = 0$ means a zero-tracking error of side-slip angle. From the time derivative of Equation 4.20, we get

$$\dot{s}_\beta = \dot{\beta} - \dot{\beta}_d \quad (4.21)$$

Using Equation 4.1 and 4.21 yields

$$\dot{s}_\beta = -\frac{2(C_f + C_r)}{mv_x}\beta + \left(\frac{2(l_r C_r - l_f C_f)}{mv_x^2} - 1\right)\gamma + \frac{2C_f}{mv_x}\delta_f - \dot{\beta}_d \quad (4.22)$$

To achieve the control requirement, a reaching surface to be satisfied is designed as follows:

$$\dot{s}_\beta = -k_{p\beta}s_\beta - k_{s\beta} \cdot sgn(s_\beta) \quad (4.23)$$

where, $k_{p\beta}$ and $k_{s\beta}$ are the parameters that follow the same rule of the inner yaw rate controller. The outer sliding mode control law γ, derived from Equations 4.22 and 4.23 is:

$$\gamma = D\left[\dot{\beta}_d + \frac{2(C_f + C_r)}{mv_x}\beta - \frac{2C_f}{mv_x}\delta_f - k_{p\beta}s_\beta - k_{s\beta} \cdot sgn(s_\beta)\right] \quad (4.24)$$

The adaptation method in Equation 4.24 without a complex design process by deriving from the equality relationship between a yaw spring coefficient A

and from the cornering stiffness C_f in Equation 4.14. Therefore, the outer sliding mode control law, Equation 4.24 can be rewritten as

$$\gamma = \hat{D}\left[\dot{\beta}_d + \frac{2\left(\hat{C}_f + \hat{C}_r\right)}{mv_x}\beta - \frac{2\hat{C}_f}{mv_x}\delta_f - k_{p\beta}s_\beta - k_{s\beta}\cdot sgn\left(s_\beta\right)\right] \quad (4.25)$$

where $\hat{C}_r$ is the estimated rear cornering stiffness and $\hat{D}$ is newly defined for the avoiding complex equation (i.e., $\hat{D} = \frac{mv_x^2}{2\hat{A}-mv_x^2}$).

To prove the stability of the outer sideslip angle control system as similar way in previous section, the positive definite V_2 is defined as

$$V_2 = \frac{1}{2}s_\beta^2 \quad (4.26)$$

$$\dot{V}_2 = s_\beta\dot{S}_\beta = S_\beta\left[-\frac{2\left(C_f + C_r\right)}{mv_x}\beta + \left(\frac{2\left(l_rC_r - l_fC_f\right)}{mv_x^2} - 1\right)\gamma + \frac{2C_f}{mv_x}\delta_f - \dot{\beta}_d\right] = S_\beta\left[-k_{p\beta}s_\beta - k_{s\beta}\cdot sgn\left(s_\beta\right)\right]$$
$$= -k_{p\beta}s_\beta - k_{s\beta}\left|s_\beta\right| < 0 \quad (4.27)$$

Therefore, the outer sliding mode control law makes the closed loop control system asymptotically stable by Lyapunov stability theory. It becomes clear that proposed all control system is asymptotically stable due to the cascade structure of the controller.

The control laws of the proposed MASMC (i.e., Equations 4.15 and 4.25) have the discontinuity term, *sgn(s)*, which may lead to the undesirable chattering problem. A solution is proposed by replacing a discontinuous switching function with a saturation function, having the boundary layer thickness Φ as the continuous approximation of a signum function as follows:

$$sgn\,(s_i) \approx sat\left(\frac{s_i}{\Phi_i}\right) = \begin{cases} \dfrac{s_i}{\Phi_i}, & if \ \left|\dfrac{s_i}{\Phi_i}\right| < 1 \\ sgn\left(\dfrac{s_i}{\Phi_i}\right), & otherwise \end{cases} \quad (i = \gamma, \beta) \qquad (4.28)$$

Finally, two types of modes can be used in the proposed MASMC owing to the cascade structure, the safety mode and fun-to-drive mode. The synthesis control scheme is shown in Figure 4.2.

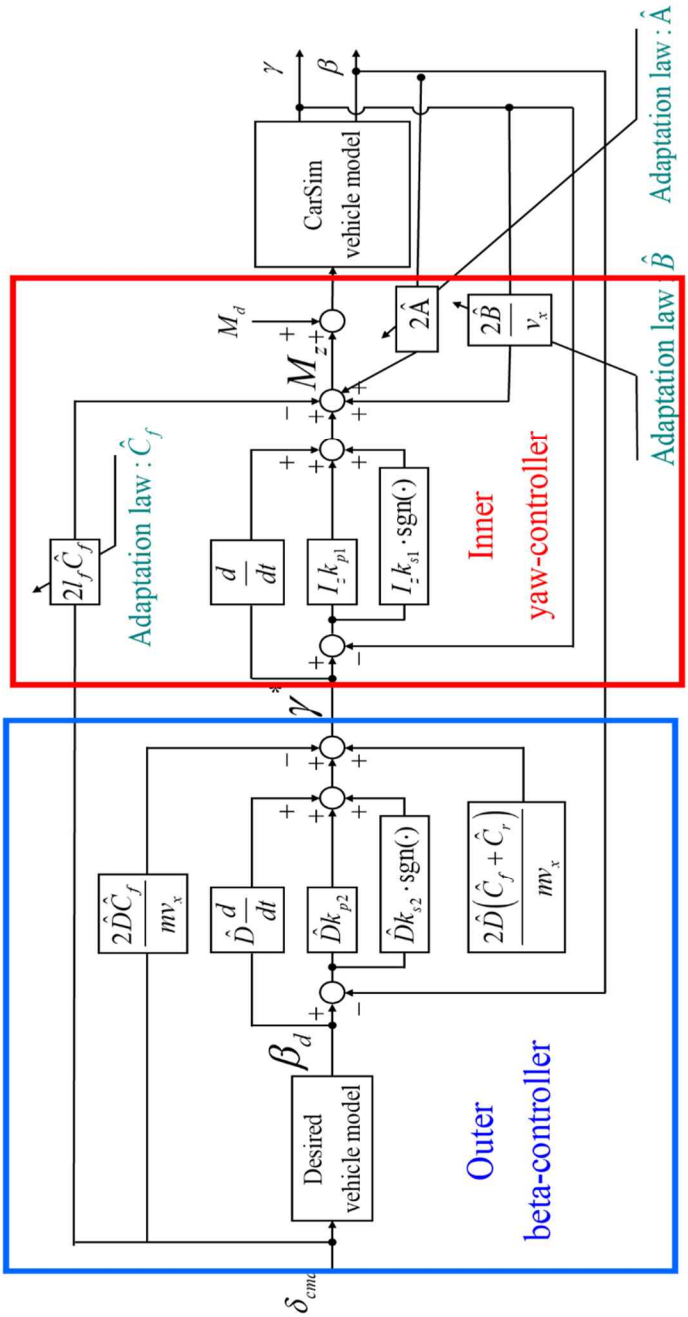

Figure 4.2 Synthesis control scheme of MASMC.

4.3. Optimal Torque Distribution (OTD)

4.3.1. Constraints of dynamics

An optimal torque distribution method that uses an active front steering system with four in-wheel- motors is described in this section. Because our system to be controlled has three control inputs and five controllable outputs, the actuator redundancy issue should be considered to avoid the saturation of driving and lateral forces [Fujimoto and Harada 2015] [Maeda, Fujimoto, and Hori 2013] [Wang et al. 2013]. The five control variables need satisfy the following equality constraints given by force and moment balance equations.

A) Longitudinal balance

The sum of the generated longitudinal tire forces on the four wheels must be equal to the required total longitudinal force to satisfy the driver's pedal command.

$$F_{cm\,d} = F_f^y \sin\delta_f + F_{fl}^x \cos\delta_f + F_{fr}^x \cos\delta_f + F_{rl}^x + F_{rr}^x \qquad (4.29)$$

B) Lateral balance

The sum of the generated lateral tire forces on the four wheels must be equal to the required total lateral force to follow the desired lateral force.

$$ma_{y,d} = F_f^y \cos\delta_f + F_r^y + F_{fl}^x \sin\delta_f + F_{fr}^x \sin\delta_f \qquad (4.30)$$

C) Moment balance

The sum of the generated moment by longitudinal and lateral tire forces must be equal to the required total yaw moment to meet desired yaw rate response.

$$M_z = l_f F_f^y \cos\delta_f - l_r F_r^y + F_{fl}^x \left(l_f \sin\delta_f - \frac{d}{2}\cos\delta_f \right) + F_{fr}^x \left(l_f \sin\delta_f + \frac{d}{2}\cos\delta_f \right) - \frac{d}{2} F_{rl}^x + \frac{d}{2} F_{rr}^x \quad (4.31)$$

Moreover, the relation between three tire forces (longitudinal tire force F_i^x, lateral tire force F_i^y and vertical tire force F_i^z) should satisfy the following equation:

$$\sqrt{F_i^{x2} + F_i^{y2}} \leq \mu_{max} F_i^z \quad (4.32)$$

From Equation 4.32, we can confirm that it is a circle which implies that the resultant force of F_i^x and F_i^y cannot exceed the maximum tire force $\mu_{max} F_i^z$. This circle is called the friction circle. The vertical tire force F_i^z is obtained from the following equations in which the effects of weight transfer according to longitudinal and lateral accelerations are described:

$$F_i^z = m\,g\left[\frac{l_r}{2l} - \frac{a_x}{g}\frac{h_{CG}}{2l} \mp \frac{a_y}{g}\frac{l_r h_{CG}}{dl}\right], i = fl, fr$$
$$F_i^z = m\,g\left[\frac{l_r}{2l} + \frac{a_x}{g}\frac{h_{CG}}{2l} \mp \frac{a_y}{g}\frac{l_r h_{CG}}{dl}\right], i = rl, rr \quad (4.33)$$

As aforementioned, the tire workload, which is the rate of the maximum tire force that can be generated in a friction circle against the current resultant force is a critical indicator of tire force saturation. The work-loads function η_i is defined as follows:

$$\eta_i = \frac{\sqrt{F_i^{x2} + F_i^{y2}}}{\mu_{max} F_i^z}, i = fl, fr, rr, rl \quad (4.34)$$

4.3.2. Optimal torque distribution law

To solve the optimization problem, the least squares method is widely used. Based on equality constraint equations 4.29, 4.30 and 4.31 and the concept of the friction circle, an optimization problem is formulated as follows:

$$\begin{aligned} &minimize \quad J \\ &subject \quad to \quad Ax = y \end{aligned} \tag{4.35}$$

where,

$$A = \begin{bmatrix} \sin\delta_f & \cos\delta_f & \cos\delta_f & 1 & 1 \\ \cos\delta_f & \sin\delta_f & \sin\delta_f & 0 & 0 \\ l_f\cos\delta_f & l_f\sin\delta_f - \frac{d}{2}\cos\delta_f & l_f\sin\delta_f + \frac{d}{2}\cos\delta_f & -\frac{d}{2} & \frac{d}{2} \end{bmatrix}$$

$$x = \begin{bmatrix} F_{f,d}^{y} & F_{fl,d}^{y} & F_{fr,d}^{y} & F_{rl,d}^{y} & F_{rr,d}^{y} \end{bmatrix}^2, y = \begin{bmatrix} F_{cm\,d} \\ ma_{y,d} - F_r^y \\ M_z + l_r F_r^y \end{bmatrix} \tag{4.36}$$

The cost function J is defined as the sum of the squares of the individual wheel's workloads as follows:

$$J = \frac{1}{2}x^T Q x = \frac{1}{2}\sum_{i=1}^{4}(\mu_{max}\eta_i) = \frac{1}{2}\sum_{i=1}^{4}\left(\frac{F_i^{x2} + F_i^{y2}}{F_i^{z2}}\right) \tag{4.37}$$

where,

$$Q = diag\left(\frac{2}{F_f^{z2}} + \frac{2\left(l_f/l_r\right)^2}{F_r^{z2}}, \frac{1}{F_{fl}^{z2}}, \frac{1}{F_{fr}^{z2}}, \frac{1}{F_{rl}^{z2}}, \frac{1}{F_{rr}^{z2}}\right) \tag{4.38}$$

Using Lagrange's theorem at the quadratic with linear constraint, the unique solution x_{opt} with respect to the optimization Equation 4.35 is obtained as follows:

$$x_{opt} = Q^{-1}A^T(AQ^{-1}A^T)^{-1}y \tag{4.39}$$

The optimal torque command to the four-in-wheel-motors is calculated as follows:

$$T_{i,d} = rF_{i,d}^{x}(i = fl, fr, rl, rr) \quad (4.40)$$

4.4. Validation with Simulation

4.4.1. Simulation setup

Two types of simulation scenarios were conducted to confirm the effectiveness of the proposed MASMC scheme. A simulation environment using the CarSim model and Matlab/Simulink was constructed for the implementation of the proposed MASMC scheme. The double-lane-change tests which is the same test scenario in Chapter 3 were carried out at v_x = 100 km/h on a high-μ road (i.e., μ = 1.0) with path following mode. Otherwise, the cornering tests, which have a 70m radius, have been done on a high-μ road (i.e., μ = 1.0) at v_x = 77 km/h with path following mode. In the simulation, to better represent actual vehicle dynamics, Magic Formula-based tire model can be used. The simulation results are obtained from four cases of control modes. The proposed MASMC is compared with results of without control, conventional lateral motion control method which is yaw tracking control with sliding mode control and the MASMC without optimal torque distribution [Goggia et al. 2014], [Nam, Fujimoto, and Hori 2015]. The specification of the simulation electric vehicle is the same as the parameters as shown in Table 3.3.

4.4.2. Simulation results

In the whole scenario, the driver attempts to follow the path by manipulating steering wheel in path following mode. Figure 4.3.– 4.6 illustrate the first

simulation scenario. These tests were performed to evaluate the transient-state performance of the proposed method. During the tests, according to Equation 4.6, a reference yaw rate was created in conventional yaw rate tracking control. The two proposed methods are compared with the conventional method with identical control gains for fair comparison.

(a)

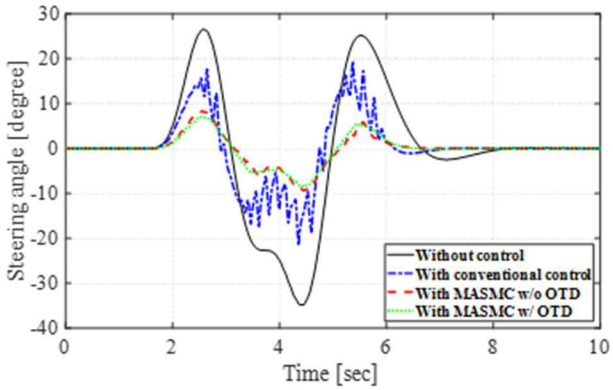

(b)

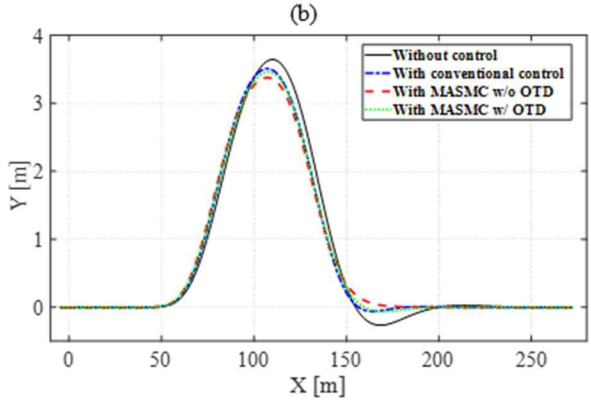

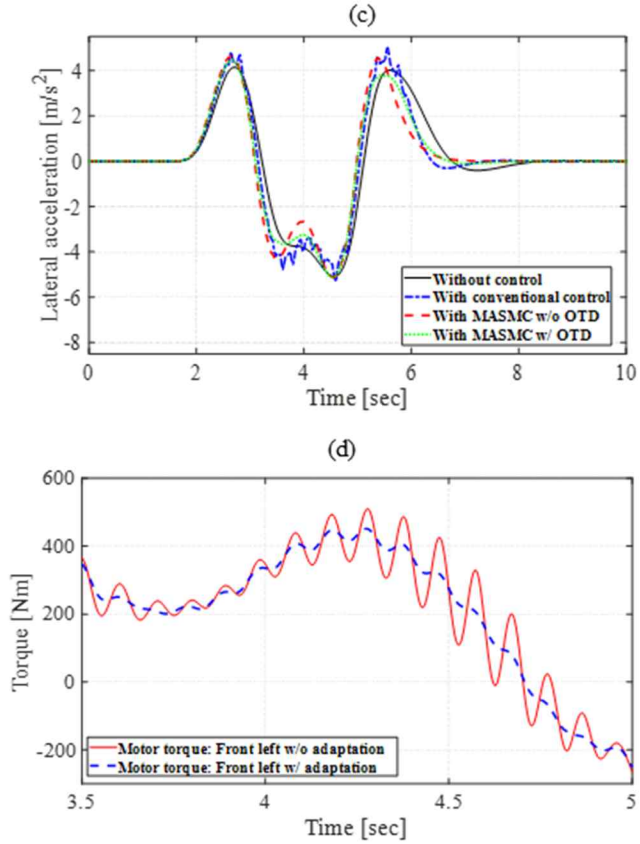

Figure 4.3. Comparison of the three different control methods on DLC test

Figure 4.3. shows the comparison results of the three control methods. The angle of the driver's steering wheel and manipulation effort, which must be reduced to improve handling performance, are shown in Figure 4.3.(a). It is validated that the manipulation effort is reduced by the proposed MASMC. The adaptation effect, which decreased the burden of saturation function, is shown

(a)

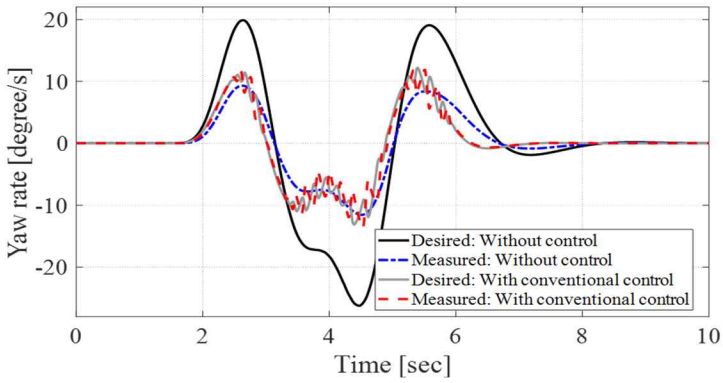
Yaw rate [degree/s]
Time [sec]
Desired: Without control
Measured: Without control
Desired: With conventional control
Measured: With conventional control

(b)

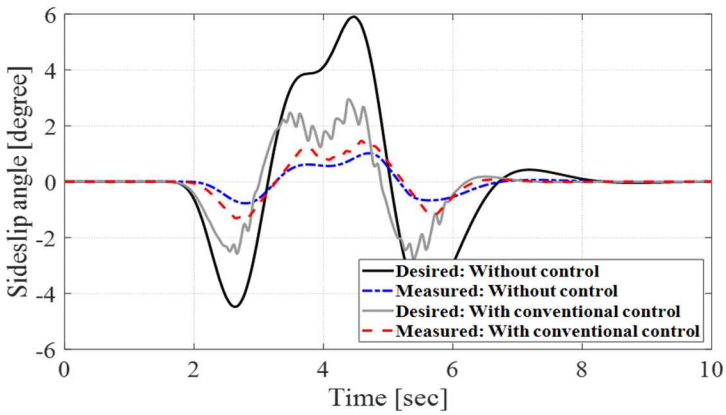
Sideslip angle [degree]
Time [sec]
Desired: Without control
Measured: Without control
Desired: With conventional control
Measured: With conventional control

(c)

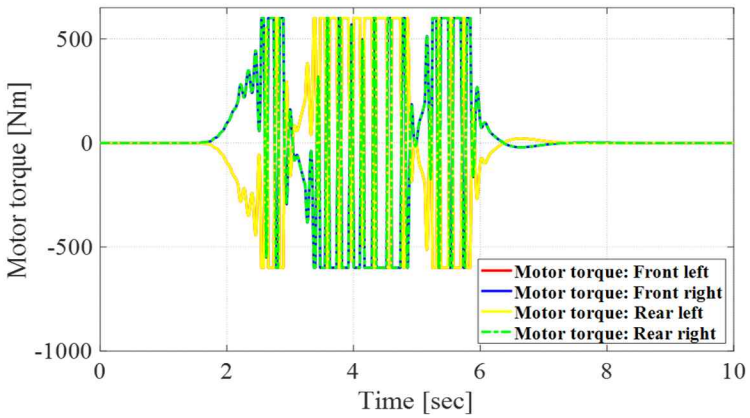
Motor torque [Nm]
Time [sec]
Motor torque: Front left
Motor torque: Front right
Motor torque: Rear left
Motor torque: Rear right

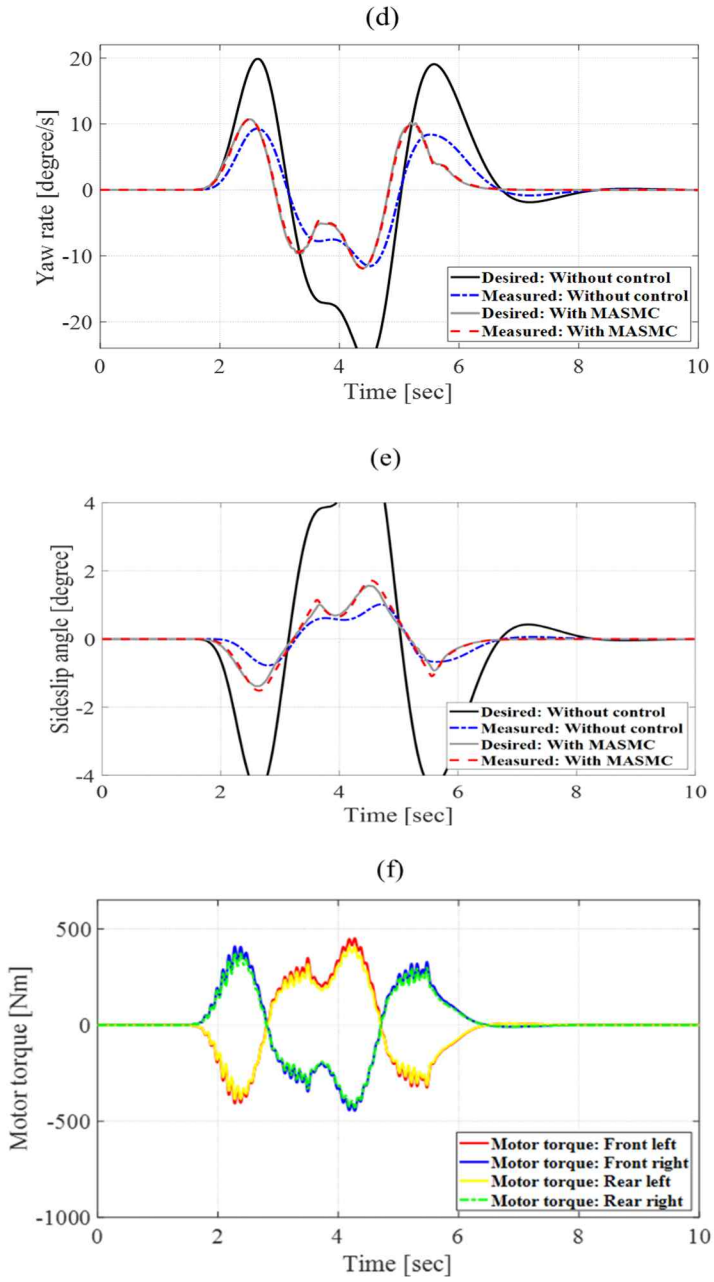

Figure 4.4 Comparison between conventional and MASMC control. (a), (b), and (c) are conventional control, (d), (e), and (f) MASMC control.

in Figure 4.3.(d). Figure 4.4 (a), (b) and (c) represent the simulation data of vehicle motion for conventional yaw tracking control, which shows good yaw rate tracking performance. Figure 4.4 (d), (e), and (f) represent those of proposed MASMC without optimal torque distribution, showing the good sideslip angle tracking performance. Figure 4.5 represents the driving data of the proposed MASMC compared to the driving data of the proposed MASMC without optimal torque distribution, seeing whether the three constraints in the previous section are satisfied. Due to the optimal torque distribution law, the input of in-wheel-motor torque's redundancy is decreased. Figure 4.7–4.10 illustrate the second simulation scenario. These tests were performed to evaluate the steady-state performance of the proposed method. We can see that the steady-state manipulation effort, which is noticeably reduced by the proposed MASMC, is shown in Figure 4.7(a).

(a)

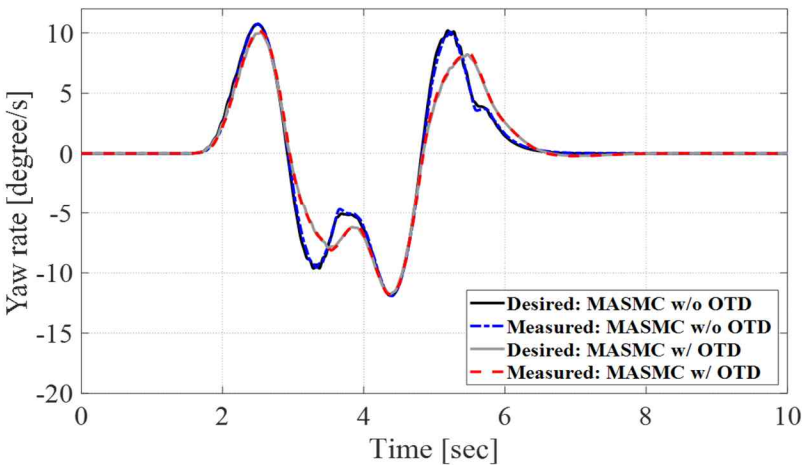

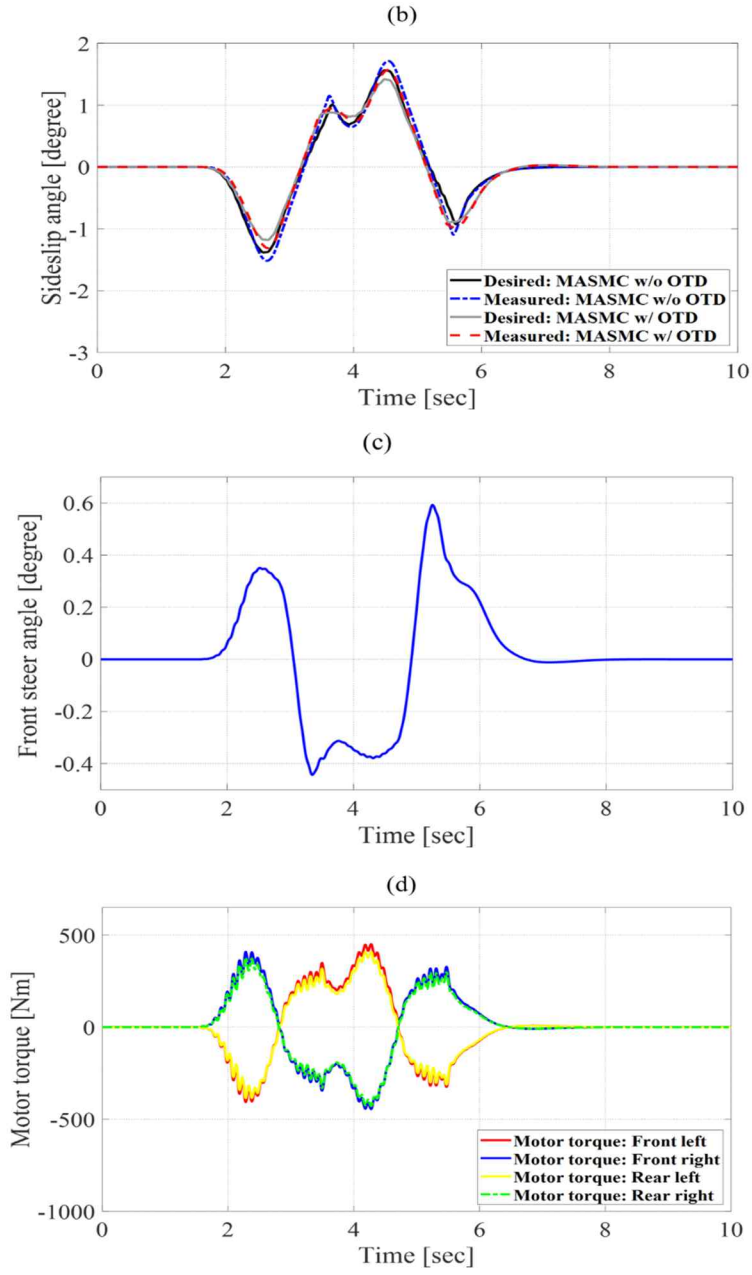

Figure 4.5 vehicle motion data of MASMC with and without OTD

The adaptation effect, which decreased the burden of saturation function, is shown in Figure 4.6(d). Figure 4.7 represents the driving data of conventional yaw tracking control, which shows the good yaw rate tracking performance. Figure 4.8 represents the driving data of the proposed MASMC without optimal torque distribution, showing the good side-slip angle tracking performance. Figure 4.9 represents the driving data of the proposed MASMC compared to the driving data of the proposed MASMC without optimal torque distribution, seeing whether the three constraints in the previous section are satisfied.

(a)

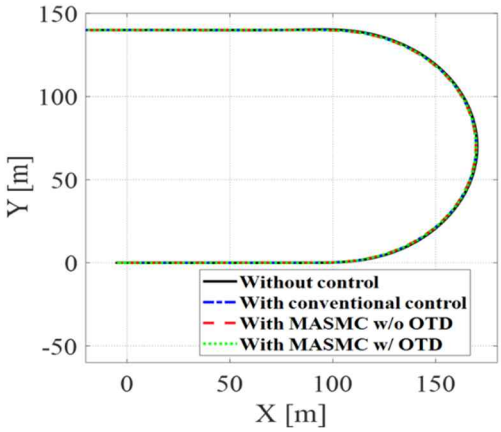

(b)

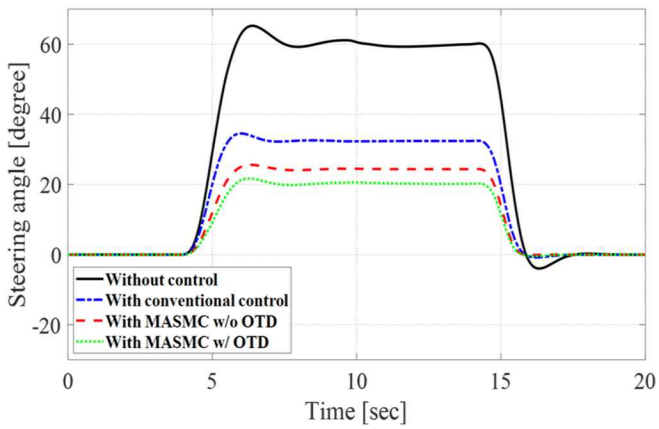

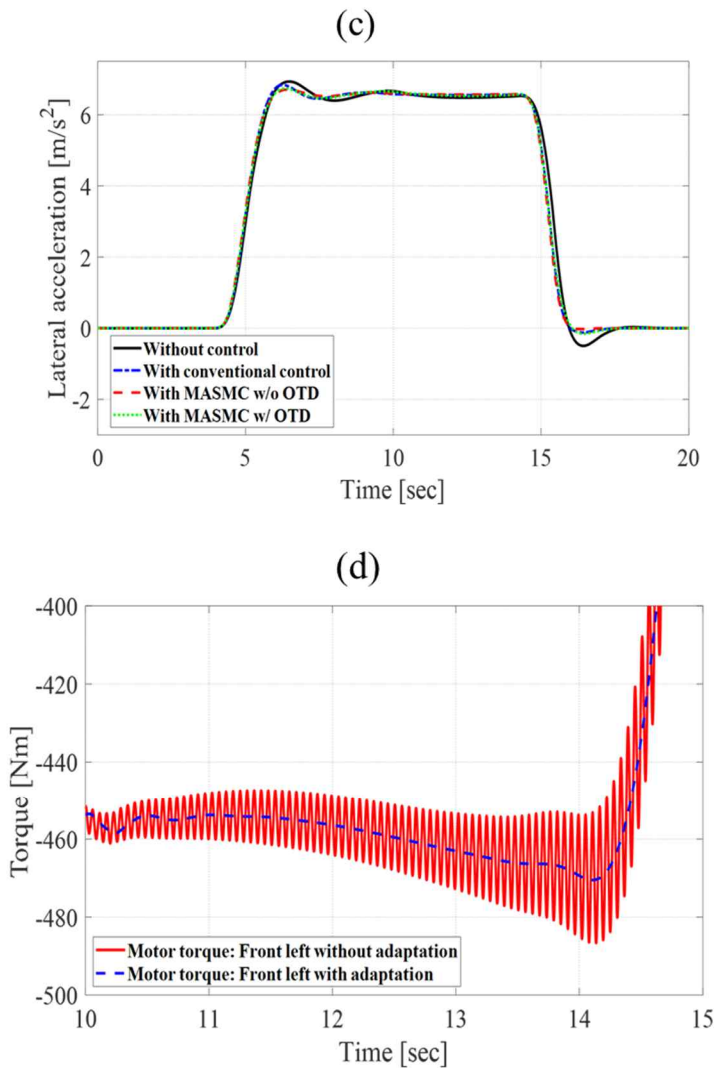

Figure 4.6 Comparison of three control methods

(a)

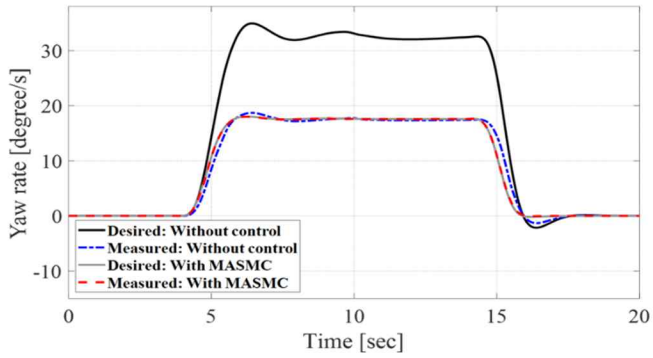

(b)

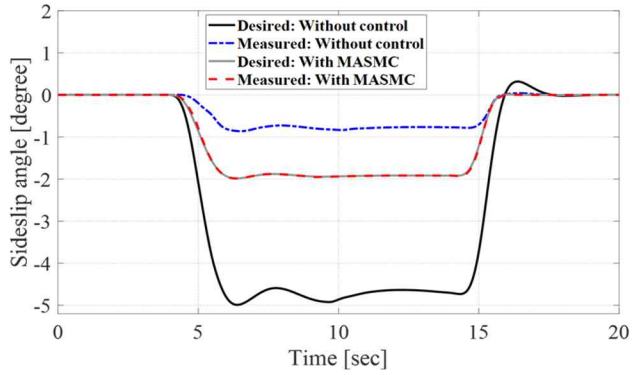

(c)

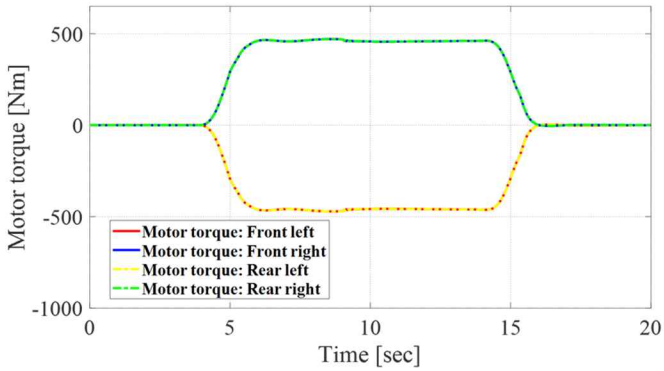

Figure 4.7 vehicle motion data of conventional control

(a)

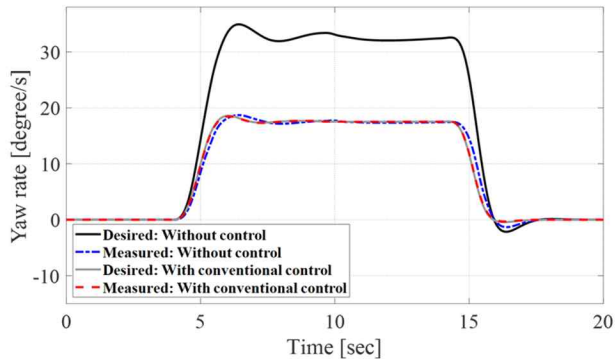

(b)

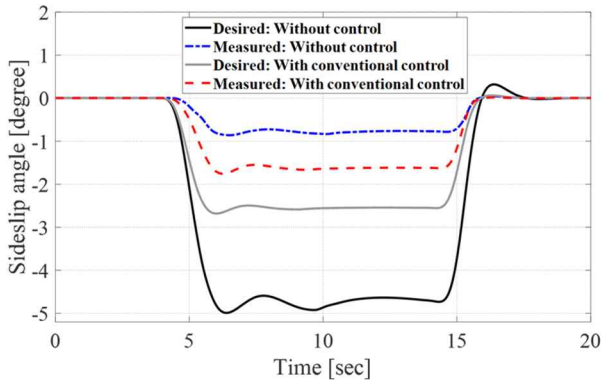

(c)

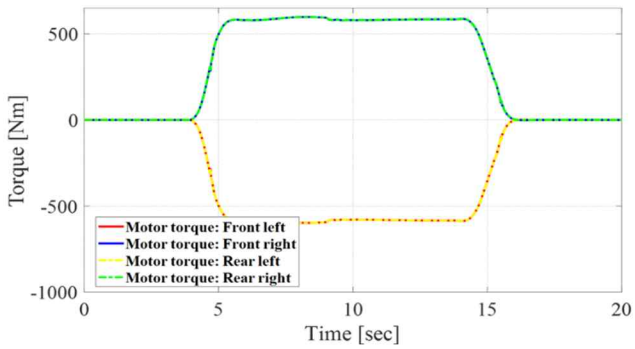

Figure 4.8 vehicle motion data of MASMC without OTD

Compared to the first simulation, the input of in-wheel motor torque redundancy is noticeably decreased by the optimal torque distribution law, which is composed of an active front steer system, as shown in Figure 4.9.

(a)

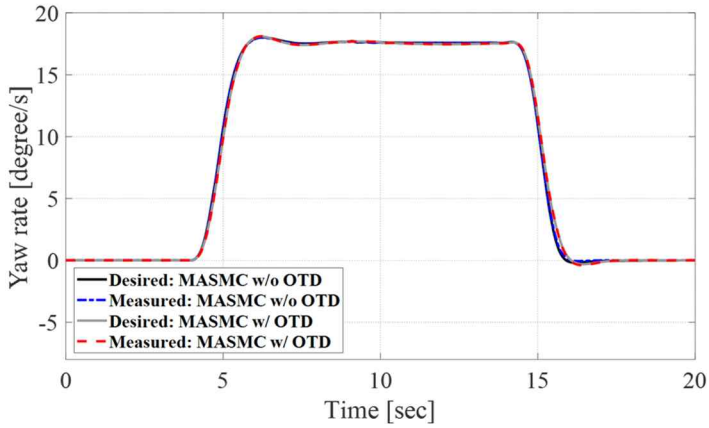

(b)

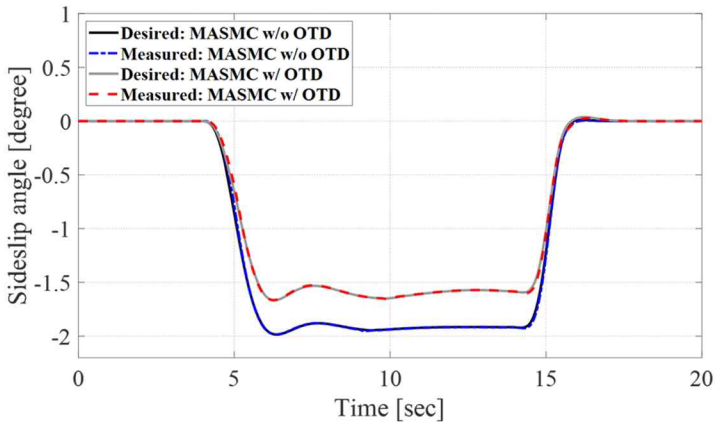

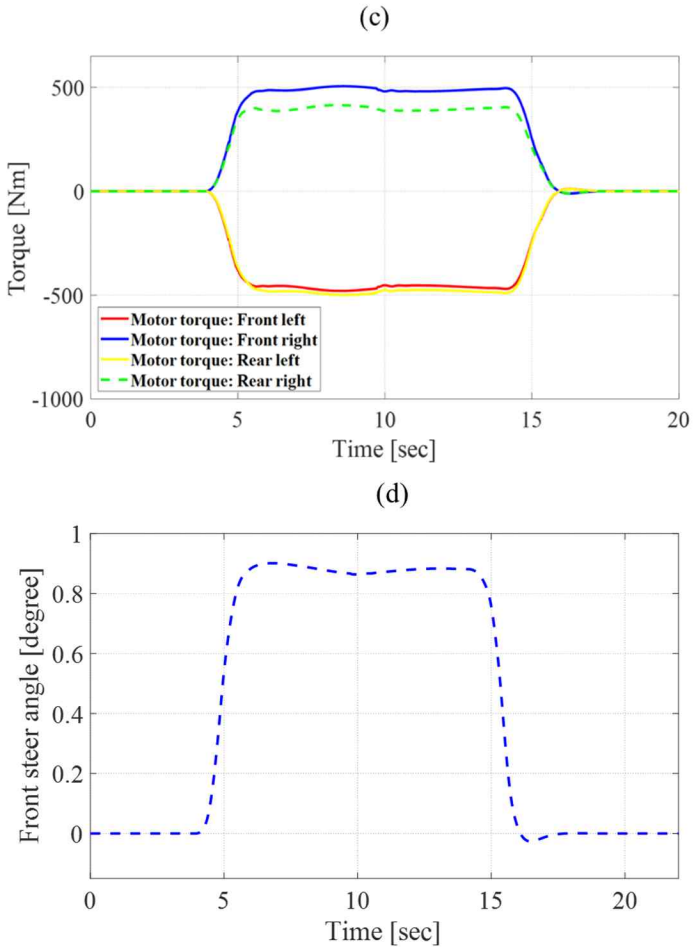

Figure 4.9 vehicle motion data of MASMC with STD

Chapter 5 Conclusion and Future works

5.1 Conclusion

This dissertation has proposed dynamic behavior based TV control methods at limit handling condition for IWMs. In Chapter 2, firstly the characteristics of vehicle dynamics in the limit handling situation has been analyzed with the grip and slip condition of the tire. The automated drift controller that tracks the state of the vehicle in the slip condition having strong nonlinear characteristics, has been developed with equalibrim analysis and discrete sliding model control. It was verified that it works well through simulation and actual vehicle experiment.. This is a study that will also be available for future self-driving vehicles, which is highly related to the condition under which the relationship between road surfaces and tires is sliped, or high-speed stability of them. Through this basic study, Dynamic TV controllers applicable to IWMs have been practically developed with dynamic nature of vehicle, understeer and oversteer. In Chapter 3, using the vehicle's inherent attribute, understeer gradient, the TV controller was designed by applying steady-state demand yaw moments in the feedforward way, and the time delay term to control the yaw damping. Therefore, the controller would be called by a dynamic TV controller. The simulation results shows that the effect of TV control on operation shows that through linear curve fittings, 63.5% of the decrease in the understeer gradient with lateral acceleration compared to base vehicles has been improved. In open loop step steer test, the yaw rate overshoot and rising time can be controllered by the gain, η with time constant of TV controller. It found that

the TV controller with two motor system in IWMs worked well for the vehicle's agileness and understeer characteristics with simulation and vehicle tests.

Another approach to control for four motor system with IWMs was formulated with yaw motion control and sideslip angle control by stages. MASMC was developed to cascade the required yaw rate and sideslip angle by adaptation law for cornering stiffness of tires that affects the value of the stability factor that contais the steering characteristics of the vehicle. The adaptaion law for cornering stiffness of tires helps reducing the chattering effects of sliding mode control. The TV control of these cascaded structures can be implemented by increasing the required side-slip angle and yaw rate for fun to drive mode pursued in this paper, and by using low target yaw rate and side-slip angle in safe mode, dynamic handling characteristics of IWMs can be created. The optimal torque distribution(OTD) method has beed used for an active front steering system with four in-wheel- motors to avoid the saturation of driving and lateral forces. Using Lagrange's theorem at the quadratic with linear constraint, the unique solution with respect to the optimization equation was developed. The proposed MASMC was compared with results of without control, conventional lateral motion control method which was yaw tracking control with sliding mode control and the MASMC without optimal torque distribution with simulation. The simulation showed that the angle of the driver's steering wheel and manipulation effort, which must be reduced to improve handling performance in double lane change maneuver. The adaptation effect, which decreased the burden of saturation function was well performed with good yaw rate tracking control. the input of in-wheel motor torque redundancy was noticeably decreased by the optimal torque distribution law.

5.2 Future works

Future works aim at advancing the proposed algorithms, which could perform successful TV control in IWMs. Regardless of the traditional ICE or the electric vehicles, it is an important issue for OEM manufacturers to provide both the pleasure and stability of driving to drivers. Thus, the proposed TV control effectively controlled the four-wheel drive, providing a safer, sometimes thrilling condition of vehicle handling. The controllers shown in Chapter 2 were verified by two motor-in-wheel motor systems, but the limits and slow response of the motor power of the system are considered to be higher performance if the actuator with higher hardware power is used. The four-motor system presented in Chapter 3 needs to be applied to the actual vehicle with optimal torque distribution and further verification of high performance. The presented controller allows the vehicle to be controlled in vehicles with motor drive with fast response characteristics in the future so that it can have various and high handling performance that it has not yet had. In addition, if driving stability of the vehicle is controlled using proposed TV control, sufficient stability can be achieved in the future, even on slippery roads such as snow and rain, and applicable in self-driving vehicles.

According to recent research, another issue with the electrification of vehicles is to improve energy efficiency. It is possible to use an optimal driving route setting algorithm that can increase the efficiency of driving energy and secure driving stability of the vehicle. Therefore, the research will be a next topic on the development of an integrated driving control algorithm for the vehicle considering TV control and the development of a torque vectoring technique to minimize the energy required for acceleration/deceleration.

Implementing energy optimization while maintaining performance during cornering driving stabilization control is considered to be an important topic for future research which developing a controller of the driving control algorithm including the consumption energy and TV considering driving and regenerative energy of vehicles.

Bibliography

Abe, Masato, Yoshio Kano, Yasuji Shibahata, and Yoshimi Furukawa. 1999. "Improvement of Vehicle Handling Safety with Vehicle Side-Slip Control by Direct Yaw Moment." *Vehicle System Dynamics* 33 (sup1): 665–79.

Beal, Craig Earl, and J Christian Gerdes. 2012. "Model Predictive Control for Vehicle Stabilization at the Limits of Handling." *IEEE Transactions on Control Systems Technology* 21 (4): 1258–69.

Cai, P, X Mei, L Tai, Y Sun, and M Liu. 2020. "High-Speed Autonomous Drifting With Deep Reinforcement Learning." *IEEE Robotics and Automation Letters* 5 (2): 1247–54.

Canale, Massimo, Lorenzo Fagiano, Antonella Ferrara, and Claudio Vecchio. 2008. "Vehicle Yaw Control via Second-Order Sliding-Mode Technique." *IEEE Transactions on Industrial Electronics* 55 (11): 3908–16.

Chen, Yan, and Junmin Wang. 2011. "Fast and Global Optimal Energy-Efficient Control Allocation with Applications to over-Actuated Electric Ground Vehicles." *IEEE Transactions on Control Systems Technology* 20 (5): 1202–11.

Cutler, M, and J P How. 2016. "Autonomous Drifting Using Simulation-Aided Reinforcement Learning." In *2016 IEEE International Conference on Robotics and Automation (ICRA)*, 5442–48. https://doi.org/10.1109/ICRA.2016.7487756.

David, J H. 2004. "Integrated Chassis Control through Coordination of Active Front Steering and Intelligent Torque Distribution." In *Proceedings of 7th International Symposium on Advanced Vehicle Control, 2004*.

Dizqah, A M, B Lenzo, A Sorniotti, P Gruber, S Fallah, and J De Smet. 2016. "A Fast and Parametric Torque Distribution Strategy for Four-Wheel-Drive Energy-Efficient Electric Vehicles." *IEEE Transactions on*

Industrial Electronics 63 (7): 4367–76. https://doi.org/10.1109/TIE.2016.2540584.

Edelberg, K, S Pan, and J K Hedrick. 2013. "A Discrete-Time Sliding Mode Formulation for Automotive Cold-Start Emission Control." In *52nd IEEE Conference on Decision and Control*, 6818–23. https://doi.org/10.1109/CDC.2013.6760969.

Fuchs, F, Y Song, E Kaufmann, D Scaramuzza, and P Dürr. 2021. "Super-Human Performance in Gran Turismo Sport Using Deep Reinforcement Learning." *IEEE Robotics and Automation Letters* 6 (3): 4257–64. https://doi.org/10.1109/LRA.2021.3064284.

Fujimoto, Hiroshi, and Shingo Harada. 2015. "Model-Based Range Extension Control System for Electric Vehicles with Front and Rear Driving–Braking Force Distributions." *IEEE Transactions on Industrial Electronics* 62 (5): 3245–54.

Gluckman, David. 2010. "What Torque Vectoring Really Means for the 2012 Ford Focus, and Why You Shouldn't Get Too Excited About It." *Car and Driver*, 2010. https://www.caranddriver.com/news/a18744957/what-torque-vectoring-really-means-for-the-2012-ford-focus-and-why-you-shouldnt-get-too-excited-about-it/.

Goggia, Tommaso, Aldo Sorniotti, Leonardo De Novellis, Antonella Ferrara, Patrick Gruber, Johan Theunissen, Dirk Steenbeke, Bernhard Knauder, and Josef Zehetner. 2014. "Integral Sliding Mode for the Torque-Vectoring Control of Fully Electric Vehicles: Theoretical Design and Experimental Assessment." *IEEE Transactions on Vehicular Technology* 64 (5): 1701–15.

Goh, Jonathan Y., and J. Christian Gerdes. 2016a. "Simultaneous Stabilization and Tracking of Basic Automobile Drifting Trajectories." *IEEE Intelligent Vehicles Symposium, Proceedings* 2016-Augus (Iv): 597–602. https://doi.org/10.1109/IVS.2016.7535448.

Goh, Jonathan Y, and J Christian Gerdes. 2016b. "Simultaneous Stabilization

and Tracking of Basic Automobile Drifting Trajectories." In *2016 IEEE Intelligent Vehicles Symposium (IV)*, 597–602. IEEE.

Hindiyeh, Rami Y, and J Christian Gerdes. 2014. "A Controller Framework for Autonomous Drifting: Design, Stability, and Experimental Validation." *Journal of Dynamic Systems, Measurement, and Control* 136 (5).

International Organization for Standardization. 2010. "Road Vehicles – Vehicle Dynamics and Road-Holding Ability – Vocabulary." In *International Organization for Standardization*. Vol. ISO Standa.

Ireson, Nelson. 2010. "Ford Focus Gets Torque Vectoring, We're Not Thrille." Motor Authority. 2010. https://www.motorauthority.com/news/1052953_2012-ford-focus-gets-torque-vectoring-were-not-thrilled.

Joa, Eunhyek, Hyunsoo Cha, Youngjin Hyun, Youngil Koh, Kyongsu Yi, and Jaeyong Park. 2020. "A New Control Approach for Automated Drifting in Consideration of the Driving Characteristics of an Expert Human Driver." *Control Engineering Practice* 96: 104293.

Joa, Eunhyek, Kwanwoo Park, Youngil Koh, Kyongsu Yi, and Kilsoo Kim. 2018. "A Tyre Slip-Based Integrated Chassis Control of Front/Rear Traction Distribution and Four-Wheel Independent Brake from Moderate Driving to Limit Handling." *Vehicle System Dynamics* 56 (4): 579–603. https://doi.org/10.1080/00423114.2017.1397276.

Kaiser, Gerd, Frédéric Holzmann, Benoît Chretien, Matthias Korte, and Herbert Werner. 2011a. "Torque Vectoring with a Feedback and Feed Forward Controller-Applied to a through the Road Hybrid Electric Vehicle." In *2011 IEEE Intelligent Vehicles Symposium (IV)*, 448–53. IEEE.

———. 2011b. "Torque Vectoring with a Feedback and Feed Forward Controller - Applied to a through the Road Hybrid Electric Vehicle." *IEEE Intelligent Vehicles Symposium, Proceedings*, no. Iv: 448–53.

https://doi.org/10.1109/IVS.2011.5940459.

Knauder, Bernhard, Dzmitry Savitski, Johan Theunissen, and Leonardo De Novellis. 2014. “Electric Torque Vectoring for Electric Vehicles.” *ATZelektronik Worldwide* 9 (4): 50–55. https://doi.org/10.1365/s38314-014-0268-0.

Koibuchi, Ken, Masaki Yamamoto, Yoshiki Fukada, and Shoji Inagaki. 1996. “Vehicle Stability Control in Limit Cornering by Active Brake.” SAE technical paper.

Liniger, Alexander, Alexander Domahidi, and Manfred Morari. 2015. “Optimization-based Autonomous Racing of 1: 43 Scale RC Cars.” *Optimal Control Applications and Methods* 36 (5): 628–47.

Lu, Qian, Pierangelo Gentile, Antonio Tota, Aldo Sorniotti, Patrick Gruber, Fabio Costamagna, and Jasper De Smet. 2016. “Enhancing Vehicle Cornering Limit through Sideslip and Yaw Rate Control.” *Mechanical Systems and Signal Processing* 75: 455–72.

Maeda, Kenta, Hiroshi Fujimoto, and Yoichi Hori. 2013. “Four-Wheel Driving-Force Distribution Method for Instantaneous or Split Slippery Roads for Electric Vehicle.” *Automatika: Časopis Za Automatiku, Mjerenje, Elektroniku, Računarstvo i Komunikacije* 54 (1): 103–13.

Milliken, William F. 1994. *Race Car Vehicle Dynamics*. *SAE International*. https://www.sae.org/publications/books/content/r-146/.

Mobis, Hyundai. 2016. “Introduction of In-Wheel System.” 2016. https://www.mobis.co.kr/communityid/9/view.do?idx=5056.

Mutoh, Nobuyoshi, Takuro Kazama, and Kazuya Takita. 2006. “Driving Characteristics of an Electric Vehicle System with Independently Driven Front and Rear Wheels.” *IEEE Transactions on Industrial Electronics* 53 (3): 803–13.

Mutoh, Nobuyoshi, and Yuki Nakano. 2011. “Dynamics of Front-and-Rear-Wheel-Independent-Drive-Type Electric Vehicles at the Time of Failure.” *IEEE Transactions on Industrial Electronics* 59 (3): 1488–99.

Nam, Kanghyun, Hiroshi Fujimoto, and Yoichi Hori. 2015. “Design of an Adaptive Sliding Mode Controller for Robust Yaw Stabilisation of in–Wheel–Motor–Driven Electric Vehicles.” *International Journal of Vehicle Design* 67 (1): 98–113.

Nam, Kanghyun, Sehoon Oh, Hiroshi Fujimoto, and Yoichi Hori. 2012. “Robust Yaw Stability Control for Electric Vehicles Based on Active Front Steering Control through a Steer-by-Wire System.” *International Journal of Automotive Technology* 13 (7): 1169–76.

Pacejka, H. 2005. *Tire and Vehicle Dynamics*. Elsevier.

Park, Kwanwoo, Eunhyek Joa, Kyongsu Yi, and Youngsik Yoon. 2020. “Rear-Wheel Steering Control for Enhanced Steady-State and Transient Vehicle Handling Characteristics.” *IEEE Access* 8: 149282–300.

Sakai, Shin-ichiro, Hideo Sado, and Yoichi Hori. 1999. “Motion Control in an Electric Vehicle with Four Independently Driven In-Wheel Motors.” *IEEE/ASME Transactions on Mechatronics* 4 (1): 9–16.

Shen, Wei, Zhichun Pan, Min Li, and Hui Peng. 2018. “A Lateral Control Method for Wheel-Footed Robot Based on Sliding Mode Control and Steering Prediction.” *IEEE Access* 6: 58086–95.

Vignati, Michele, Edoardo Sabbioni, and Davide Tarsitano. 2016. “Torque Vectoring Control for IWM Vehicles.” *International Journal of Vehicle Performance* 2 (3): 302–24.

Voser, Christoph, Rami Y Hindiyeh, and J Christian Gerdes. 2010. “Analysis and Control of High Sideslip Manoeuvres.” *Vehicle System Dynamics* 48 (S1): 317–36.

Vossler, Chuck. 2014. “Winter Driving Settings in Your BMW – Editorial.” BMWBLOG. 2014. https://www.bmwblog.com/2014/02/16/winter-driving-settings-bmw-editorial/.

Wang, Rongrong, Hamid Reza Karimi, Nan Chen, Guodong Yin, and Jinxiang Wang. 2013. “Motion Control of Four-Wheel Independently Actuated Electric Ground Vehicles Considering Tire Force Saturations.”

Mathematical Problems in Engineering 2013.

Wang, Rongrong, and Junmin Wang. 2011. “Fault-Tolerant Control with Active Fault Diagnosis for Four-Wheel Independently Driven Electric Ground Vehicles.” *IEEE Transactions on Vehicular Technology* 60 (9): 4276–87.

Williams, Daniel E, and Wassim M Haddad. 1995. “Nonlinear Control of Roll Moment Distribution to Influence Vehicle Yaw Characteristics.” *IEEE Transactions on Control Systems Technology* 3 (1): 110–16.

Yang, Derong, Martin Idegren, and Mats Jonasson. 2018. “Torque Vectoring Control for Progressive Cornering Performance in AWD Electric Vehicles.” In *Proceedings of AVEC*.

Yin, Dejun, Sehoon Oh, and Yoichi Hori. 2009. “A Novel Traction Control for EV Based on Maximum Transmissible Torque Estimation.” *IEEE Transactions on Industrial Electronics* 56 (6): 2086–94.

Zanten, Anton T Van. 2002. “Evolution of Electronic Control Systems for Improving the Vehicle Dynamic Behavior.” In *Proceedings of the 6th International Symposium on Advanced Vehicle Control*, 2:9. Citeseer.

초 록

고성능 한계 핸들링을 위한 인휠 모터 토크벡터링 제어

지난 10년 동안 차량 자세 제어시스템(ESC)은 치명적인 충돌을 방지하기 위해 많은 상용 차량에서 비약적으로 발전되고 개발되고 있다. 특히, 차량 자세 제어 시스템은 악천후로 인한 미끄러운 도로와 같은 위험한 도로에서 불안정한 차량 주행 조건에서 사고를 피하는데 큰 역할을 한다. 그러나, 최근의 경우, 고성능 차량 또는 스포츠카 등의 경우 제동제어의 빈번한 개입은 운전의 즐거움을 감소시키는 불만도 존재한다.

최근 차량의 전동화와 함께, 자량 자세 제어시스템의 작동 영역인 한계 주행 핸들링 조건에서 각 바퀴의 휠의 독립적인 구동을 적용할 수 있는 시스템 중 하나인 인휠 모터 시스템을 사용하여 차량의 종, 횡방향 특성을 제어 가능하게 하는 토크벡터링 제어기술에 대한 연구가 활발하다. 따라서, 본 연구에서는 차량의 선회 한계 핸들링 조건에서 안정성과 주행 다이나믹 성능을 향상시킬 수 있는 토크벡터링 제어기를 제안하고자 한다. 먼저, 차량의 비선형 주행 구간인 한계 핸들링 조건에 대한 자동 드리프트 제어 알고리즘을 제안한다. 이 알고리즘을 이용하여 토크벡터링 제어에 차량의 다이나믹한 주행모드에 대한 통찰력을 제공하고 미끄러운 도로에서 차량의 높은 슬립 각도의 안정성 제어를 제공할 수 있다.

또한, 인휠 모터 시스템을 차량의 전륜에 2개 모터로 사용하여 차량 고유의 특성인 차량 언더스티어 구배를 직접적 제어를 수행하여, 차량의 핸들링 성능을 향상시켰다. 제어기의 채터링 효과를 줄이고 빠른 응답을 얻기 위해 새로운 과도 매개 변수가 이용하여 수식화 하여 구성하였으며, 차량의 정상 상태 및 과도 특성 향상을 검증하기 위하여 ISO 기반 시뮬레이션 및 차량 실험을 수행하였다. 마지막으로 요 제어기와 횡 슬립 각도 제어기로 구성된 MASMC (Multiple Adaptive Sliding Mode Control) 접근 방식을 사용하는 4륜 모터 시스템을 사용한 동적 토크벡터링 제어를 수행하였다. 높은 비선형 특성을 가진 차량의 전 후륜 타이어의 코너링 강성은 적응 제어기법을 이용하여 예측하였다. 따라서, 안전모드와 다이나믹 모드를 구성하여, 운전자로 하여금 원하는 주행의 조건에 맞게 선택할 수 있는 알고리즘을 구현하였다. 이 MASMC 알고리즘은 향후 전동화 차량에 주행안정성 향상과 다이나믹한 주행의 즐거움을 주는 기술로써, 전 차량 시뮬레이션을 이용하여 검증하였다.

주요어 : 토크벡터링제어, 인휠모터시스템, 전기차. 자율드리프트제어, 자율주행시스템, 적응제어, 슬라이딩모드제어, 비선형제어

학 번 : 2016-35616